Aus dem Max-Planck-Institut für Kolloid- und
Grenzflächenforschung

Static and dynamic properties of soluble surfactants at the air/water interface

Dissertation

zur Erlangung des akademischen Grades
"doctor rerum naturalium"
(Dr. rer. nat.)
in der Wissenschaftsdisziplin Experimentalphysik

eingereicht an der
Mathematisch-Naturwissenschaftlichen Fakultät
der Universität Potsdam

von
Patrick Kölsch,

Potsdam, April 2005

Contents

Preface

Amphiphilic molecules contain a hydrophilic headgroup and a hydrophobic tail. The headgroup is polar or ionic and likes water, the tail is typically an aliphatic chain that cannot be accommodated in a polar environment. The prevailing molecular asymmetry leads to a spontaneous adsorption of amphiphiles at the air/water or oil/water interfaces. As a result, the surface tension and the surface rheology is changed. Amphiphiles are important tools to deliberately modify the interfacial properties of liquid interfaces and enable new phenomena such as foams which cannot be formed in a pure liquid.

In this thesis we investigate the static and dynamic properties of adsorption layers of soluble amphiphiles at the air/water interface, the so called Gibbs monolayers. The classical way for an investigation of these systems is based on a thermodynamic analysis of the equilibrium surface tension as a function of the bulk composition in the framework of Gibbs theory. However, thermodynamics does not provide any structural information and several recent publications challenge even fundamental text book concepts[1].

The experimental investigation faces difficulties imposed by the low surface coverage and the presence of dissolved amphiphiles in the adjacent bulk phase. In this thesis we used a suite of techniques with the sensitivity to detect less than a monolayer of molecules at the air-water interface. Some of these techniques are extremely complex such as infrared visible sum frequency generation (IR-VIS SFG) spectroscopy or second harmonic generation (SHG). Others are traditional techniques, such as ellipsometry employed in new ways and pushed to new limits. Each technique probes selectively different parts of the interface and the combination provides a profound picture

[1]The journal Science lists this topic in the December issue of the year 2004 as one of the scientific highlights.

of the interfacial architecture.

The first part of the thesis is dedicated to the distribution of ions at interfaces. Adsorption layers of ionic amphiphiles serve as model systems allowing to produce a defined surface charge. The charge of the monolayer is compensated by the counterions. Gouy and Chapman were the first who treated this problem in a quantitative fashion. The ions were considered as point charges embedded in a continuum of a constant dielectric constants. The combination of the Boltzmann distribution with the Poisson equation leads to a nonlinear second order differential equation for the electric potential and the ion distribution at the interface.

The Gouy-Chapman theory predicts unrealistic high concentrations of counterions in the vicinity of the interface due to a neglect of the geometrical dimensions of the counterions. To overcome this difficulty, Stern divided the interfacial architecture in two distinct regions, a layer of directly bound counterions which are effectively reducing the surface charge and a diffuse layer where the counterions can move freely.

The classical theory accounts only for electrostatics and thermal motion and does not describe the huge amount of experimentally observed ion specific effects. The finding of a universal theory accounting for the various effects is one of the central topics of physical chemistry today. Several extensions to the classical theory are aiming to include dispersion forces, fluctuation, hydration, ion size effects or the impact of interfacial water in the framework of mean-field PB theory, recent contributions go beyond the mean field level. Chapter 1.1 gives an overview about the theories and underlying concepts.

The decisive information is contained in the ion distribution, however, its experimental determination is a big scientific challenge. We could demonstrate that a combination of linear and nonlinear techniques gives direct insights in the prevailing ion distribution. Our formalism does not contain any free parameter and is discussed in detail in chapter 2.4.4. Our investigations reveal specific ion effects which cannot be described by Poisson-Boltzmann mean field type theories and are discussed in chapter 3.1.

Water is a dipole and shows a preferential orientation within an electrical field. IR-VIS SFG spectroscopy probes the oriented water dipoles. Therefore investigations of the arrangement of water molecules at interfaces deliver insights in the local ion distribution. This concept is outlined in chapter

3.1.5.

Adsorption layer and bulk phase are in thermodynamic equilibrium, however, it is important to stress that there is a constant molecular exchange between adsorbed and dissolved species. This exchange process is a key element for the understanding of some of the thermodynamic properties. An excellent way to study Gibbs monolayers is to follow the relaxation from a non-equilibrium to an equilibrium state. Upon compression amphiphiles must leave the adsorption layer and dissolve in the adjacent bulk phase. Upon expansion amphiphiles must adsorb at the interface to restore the equilibrium coverage. Obviously the frequency of the expansion and compression cycles must match the molecular exchange processes. At too low frequencies the equilibrium is maintained at all times. If the frequency is too fast the system behaves as a monolayer of insoluble surfactants. In chapter 2.5 of this thesis we describe an unique variant of an oscillating bubble technique that measures precisely the real and imaginary part of the complex dilational modulus E in a frequency range up to 500 Hz. The extension of about two decades in the time domain in comparison to the conventional method of an oscillating drop is a tremendous achievement. The high frequency limit of the module is now experimentally accessible. The imaginary part of the complex dilational modulus E is a consequence of a dissipative process which is interpreted as an intrinsic surface dilational viscosity κ.

The IR-VIS SFG spectra of the interfacial water provide a molecular interpretation of the underlying dissipative process. The findings are discussed in section 3.2.4

Own papers regarding ion distribution at charged interfaces:

- An Experimental Route to Hofmeister
  Koelsch, P.; Motschmann, H.
  Current Opinion in Colloid and Interface Science, 9 (2004) 87-91.

- A Method for Direct Determination of the Prevailing Counterion Distribution at a Charged Surface
  Koelsch, P.; Motschmann, H.
  J. Phys. Chem. B 2004, 108(48),18659-18664.

- Varying the Counterions at a Charged Interface
  Koelsch, P.; Motschmann, H.
  Langmuir, in press

- Interfacial Water - a Sensitive Probe for the Distribution of Counterions
  Koelsch, P.; Motschmann, H.
  Langmuir, submitted

- Surface Selective Spectroscopy and Molecular Dynamics Simulations of Aqueous Ionic and Complementary Zwitterionic Surfactants
  P. Koelsch, H. Motschmann, M. Petrov, B. Minofar, L. Vrbka,
  P. Jungwirth
  Manuscript

Own papers regarding foam stability:

- Relating Foam Stability and Surface Rheology
  Koelsch, P.; Motschmann, H.
  Langmuir, submitted

- Understanding the Molecular Origin of Foam Stability
  Koelsch, P.; Motschmann, H.
  J. Phys. Chem. B, submitted

Other contributions as a PhD student:

- New Insights in Static and Dynamic Properties of Soluble Monolayers
  V. Fazio, J. Oertegren, P. Koelsch, A. Andersen, D. Wantke, H. Moehwald, H. Motschmann
  Proc. SPIE Vol. 5223, p. 38-48, Physical Chemistry of Interfaces and Nanomaterials II; Tianquan Lian, Hai-Lung Dai; Eds., Date: Dec 2003

- Following fast Adsorption Processes with Surface Plasmon Spectroscopy: Reflectivity versus Mismatch Tracking
  M. Schneider, A. Andersen, P. Koelsch, H. Motschmann
  Sensor and Actuators B: Chemical, Volume 104, Issue 2, 24 January 2005, 276-281

As a diploma student:

- Effect of temperature on the dynamic contact angle
  M. de Ruijter, P. Kölsch, M. Vou, J. De Coninck, J.P. Rabe
  Colloids and Surfaces A, 144 (1998) 235-243

- Novel scanning near-field optical microscope (SNOM)/scanning confocal optical microscope based on normal force distance regulation and bent etched fiber tips
  J. F. Wolf, P. E. Hillner, R. Bilewicz, P. Kölsch, J. P. Rabe
  Review of Scientific Instruments, 70 (1999) 2751-2757

Chapter 1

Scientific Questions

1.1 Ion distribution at charged interfaces

1.1.1 Introduction

The distribution of ions at a charged aqueous interface is a fundamental topic in colloid and interface science. The complex interplay of electrostatics, dispersion forces, thermal motion, fluctuation, 2D correlations, hydration and the impact of the interfacial hydrogen bonding network is only beginning to be addressed in molecular level experiments and theories [1, 2]. Molecular dynamics simulations taking into account the structure of water molecules show distinct differences in the distribution of counter-ions whether or not the polarization of water molecules is included [4, 3, 5]. Infrared-visible sum frequency generation (IR-VIS SFG) offers the possibility to investigate the bonding and structure of the interfacial water [6, 8]. Charged surfactants lead to a different vibronic water signature than uncharged amphiphiles [7, 9]. Linear and nonlinear optical techniques are probing different elements of the interfacial architecture giving insights in the ion distribution [10, 11, 12]. All these recent advances are the driving force for the renaissance in studying ions at interfaces.

The classical treatment is based on the Poisson-Boltzmann equation. Several extensions of the original theory have been proposed leading to a zoo of decorations of the original differential equations [13]. Some modern theories go beyond the mean field level and the explicit consideration of fluctuations

predicts a phase transition towards a condensed state of ions with increasing surface charge [14, 15]. This surface phase transition is questioned in [16, 17] because it is not observed in Monte Carlo simulations. Due to the inherent complexity the combination of several surface sensitive techniques is required for gaining reliable experimental data suitable for a comparison with the theories and simulations.

Adsorption layers of ionic soluble surfactants are ideal experimental model systems for studying charged aqueous interfaces. Bulk and surface layer are in thermodynamic equilibrium with a dynamic exchange of the surfactant [18]. The surface coverage is determined by the bulk concentration. The corresponding surface charge produces an electric field which is screened by the oppositely charged counter-ions.

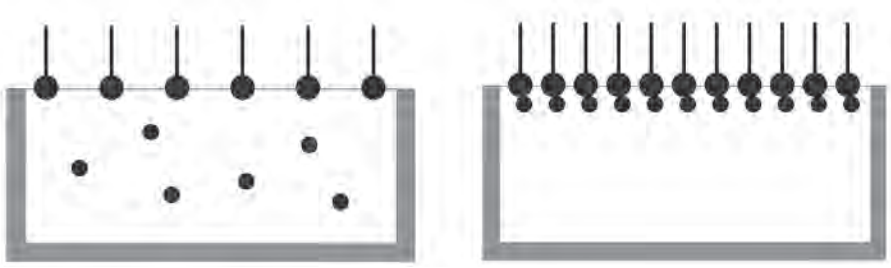

Figure 1.1: Adsorption layers of soluble ionic surfactants are well-defined model systems for studying charged aqueous interfaces. By varying the concentration of surfactants below the critical micelle concentration (cmc) one can change the adsorbed amount of surfactants at the interface and therefore the bare surface charge.

In this thesis it is demonstrated that the combination of sophisticated nonlinear (surface Second Harmonic Generation - SHG) and linear optical techniques (Ellipsometry) allows a direct determination of the prevailing ion distribution. Each technique probes different structural elements and the combination of all techniques provides a profound picture of the interfacial architecture. A simple analytical expression is derived which can be used to retrieve the number of condensed counterions within the compact or so called Stern-layer. The combined data show the existence of a phase transition between a free and a condensed state of the counterions induced by a small increase of surface charge. Additionally the influence of different counterions

on the adsorption behavior of soluble surfactants where investigated. It is shown that for cationic surfactants addition of bromide and chloride leads to a condensed state at all surfactant concentrations whereas for fluoride the phase transition occurs at decreased concentrations consistent with molecular dynamics simulations.

Water is an electrical dipole and adopts a preferential orientation within the local electric field. In a first approximation the distribution is given by a Langevin function [19]. Hence, the polar order of the water is a sensitive probe of the electric field and allows direct conclusions about the prevailing ion distribution. Our experiments take advantage of this relation. Infrared-visible sum frequency generation (IR-VIS SFG) spectroscopy measures only the oriented part of the water molecules. By further analyzing the structure of water with IR-VIS SFG spectroscopy the important role of water at charged interfaces was explored. We followed the changes in the bound and unbound OH-stretch modes by varying the amount of counterions in the solution. The IR-VIS SFG spectra confirm the existence of a phase transition in the distribution of the counterions to a condensed state.

1.1.2 The distribution of counterions for insoluble ionic surfactants

Consider a flat charged interface between air and an aqueous solution with a surface charge density σ. This situation can be obtained by nonsoluble adsorption layers of ionic surfactants. At temperature $T = 0$ all ions are condensed at the interface as a consequence of the electrostatic binding. At room temperature the electrochemical potential μ_i of the i-th ion is defined as $\mu_i = eZ\psi + k_BTln(n_i)$, where the first term is the electrostatic contribution (e = electronic unit charge, Z = valence, ψ = electric potential) and the second one (k_BT = thermal energy, n = number density) comes from the (ideal) entropy of the ions in the weak solution limit. In thermal equilibrium μ_i remains constant throughout the system. Consequently, each sort of ion i obeys a Boltzmann distribution in the solution. Recall that the combination of the Boltzmann distribution with the Poisson equation leads to a nonlinear second-order differential equation for the electric potential ψ[1] :

[1]The following representation is done in the cgs-system

$$\frac{\partial^2\psi(z)}{\partial z^2} = -\frac{4\pi e}{\epsilon_w} Z \exp\left(\frac{-eZ\psi(z)}{k_B T}\right) \tag{1.1}$$

where ϵ_w is the dielectric constant of the aqueous solution and z is the distance to the interface.

The solution of eq 1.1 reveals the number density of the counterions as a function of the distance to the interface:

$$n(z) = \frac{1}{2\pi Z^2 l_B} \frac{1}{(z+b)^2} \tag{1.2}$$

The number density decays to zero algebraically with the characteristic Gouy-Chapman (GC) length $b = e/2\pi\,|\sigma|\,l_B = \epsilon_w k_B T/2\pi e\,|\sigma|$, where $l_B = e^2/\epsilon_w k_B T \approx 7$ Å is the Bjerrum length in water at room temperature. The GC length defines a sheath near the charged surface in which most of the counterions are confined. The physical meaning of the Gouy-Chapman length becomes obvious by the integrated amount of counterions (per unit area) attracted to the surface from $z = 0$ to $z = b$, which is $-\sigma/2$. Namely, it balances half of the surface charge. Typically it is on the order of a few angstroms for $\sigma = e/100$ Å^{-2}. Note that the GC length is only a function of the surface charge density at room temperature.

1.1.3 The distribution of counterions for soluble ionic surfactants

Consider that the flat charged surface consists of an adsorbed layer of soluble ionic surfactants. The profile of the counter-ion distribution in the solution is decreasing with increasing depth until it reaches the concentration of the bulk. The situation is described by the Poisson-Boltzmann (PB) equation for a symmetric electrolyte solution:

$$\begin{aligned}\frac{\partial^2\psi(z)}{\partial z^2} &= -\frac{4\pi e n_0}{\epsilon_w} Z \left(\exp\left(\frac{eZ\psi(z)}{k_B T}\right) - \exp\left(\frac{-eZ\psi(z)}{k_b T}\right)\right) \\ &= -\frac{8\pi e n_0}{\epsilon_w} Z \sinh\left(\frac{eZ\psi(\vec{r})}{k_b T}\right)\end{aligned} \tag{1.3}$$

where n_0 is the bulk concentration. In the following we treat monovalent ions ($Z = 1$). Divalent ions have important consequences for example on the electrostatics of membranes. Most of those consequences go beyond the continuum approach of the PB theory and are discussed in [21, 28].

For surface potentials less than 25 mV at room temperature we can expand the right side of eq 1.3 to the first order in ψ:

$$\nabla^2\psi(\vec{r}) = \lambda_D^{-2}\psi(\vec{r}) \tag{1.4}$$

with

$$\lambda_D^{-2} = \sqrt{\frac{8\pi e n_0}{\epsilon_w k_B T}} \tag{1.5}$$

λ_d is the so called Debye-Hückel screening length. The electrostatic potential is exponentially screened and can be neglected for lengths larger than the Debye-Hückel screening length. λ_D is a function of the bulk concentration and on the order of a few nanometers for millimolar solutions. A solution of the PB eq 1.3 for the potential ψ under the boundary condition of a flat charged membrane with a surface charge density σ at $z = 0$ and vanishing potential at $n(\infty) = n_0$ is [23]:

$$\psi(z) = \frac{2k_B T}{e} \ln\left(\frac{1+\gamma e^{\frac{-z}{\lambda_d}}}{1-\gamma e^{\frac{-z}{\lambda_d}}}\right) = \frac{4k_B T}{e} \operatorname{arctanh}\left(\gamma e^{\frac{-z}{\lambda_d}}\right) \tag{1.6}$$

where the parameter γ is the positive root of the quadratic equation

$$\gamma^2 + \frac{2b}{\lambda_d}\gamma - 1 = 0. \tag{1.7}$$

Hence γ depends on the relation between the Gouy-Chapman and the Debye-Hückel screening length and is consequently a function of the surface charge density σ and the bulk concentration n_0. The parameter γ adopts values between 0 and 1.

The situation is plotted in Figure 1.2 for a value of $\gamma = 0.56$, which corresponds to a surface charge density of $\sigma = 0.385$ e/nm^2 and a bulk concentration of $n_0 = 0.1$ M. There is a distinct difference in the distribution

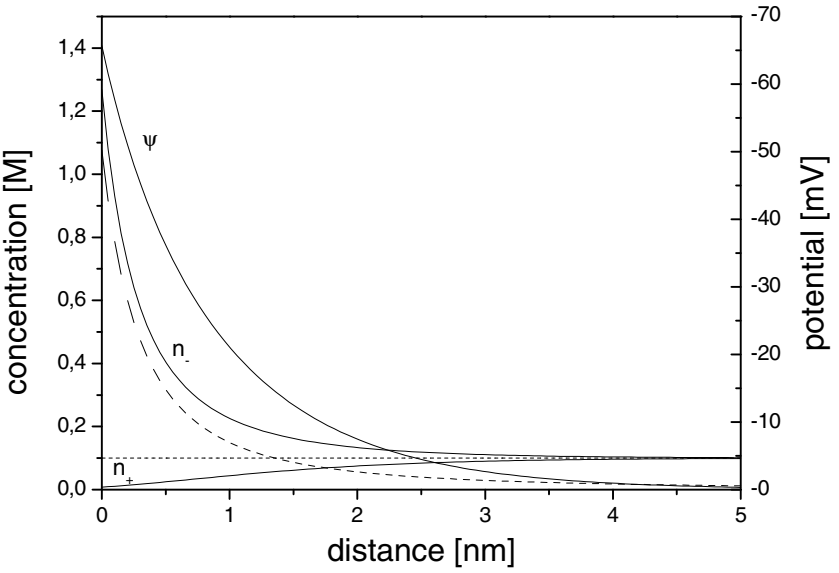

Figure 1.2: Surface potential and concentration as function of the distance from the air/water interface. A surface charge density of $\sigma = 0.385e/\text{nm}^2$ and a bulk concentration of 100 mM was used for the calculations. The dashed line displays the distribution of the counterions under the assumption that there are no co-ions in the solution. In this concentration regime an influence of the co-ions on the prevailing distribution of the counterions is observed.

of the counterions with or without co-ions in the solution. At a similar surface charge density but an essentially lower bulk concentration of $n_0 = 0.3$ mM the parameter γ is 0.9. The results of the calculations are shown in Figure 1.3. In this case the counterion distribution is not influenced by the presence of the co-ions. For values of $\gamma > 0.8$ the distribution of the counterions can be described in the same fashion for Gibbs and Langmuir layers. It is therefore justified to use eq 1.2 for the number density as a function to the distance to the surface.

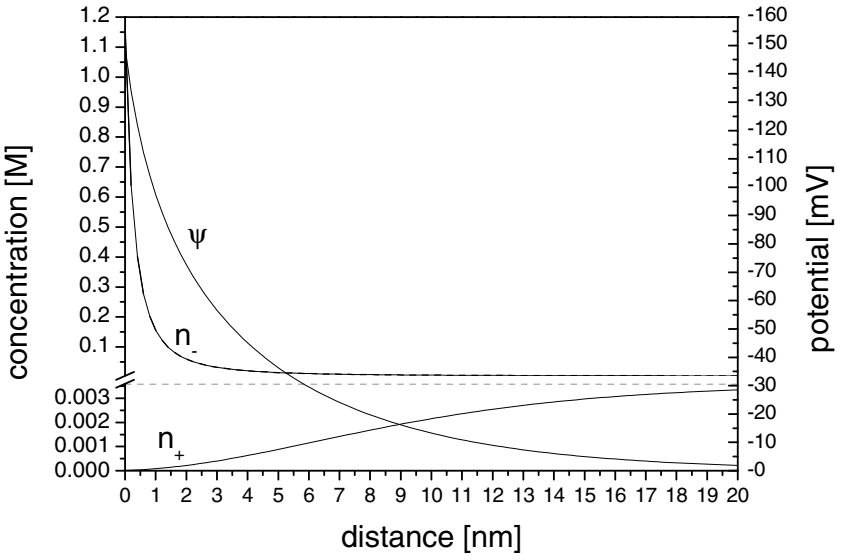

Figure 1.3: Surface potential and concentration as function of the distance from the air/water interface. A surface charge density of $\sigma = 0.385e/\mathrm{nm}^2$ and a bulk concentration of $n_0 = 3$ mM was used for the calculations. The dashed line displays the distribution of the counterions under the assumption that there are no co-ions in the solution. In this concentration regime the presence of co-ions does not influence the prevailing distribution of the counterions.

1.1.4 Beyond the mean-field approach

The shortcomings of the Gouy-Chapman theory were obvious from the beginning and Stern was the first who noticed that this theory predicts unrealistic high concentration of counterions in the vicinity of the interface due to a neglect of the geometrical dimensions of the ions [24]. He bridged this discrepancy by the division of the interfacial architecture in two distinct regions, a layer of directly bound counterions and a diffuse layer where the counterions can move freely. The directly bound counterions effectively reduce the surface charge density σ_0:

$$\sigma_{\mathrm{net}} = \sigma_0 - en_c \tag{1.8}$$

where n_c is the number density of the condensed counterions. The net surface charge density σ_{net} effectively determines the counterion distribution in the diffuse layer according to the PB theory. This approach appears to be rather artificial, however, it turns out that profiles of sophisticated molecular dynamics simulations can be mapped in a corresponding Stern-Gouy Chapman profile [20, 21]

The classical theory accounts only for electrostatics and thermal motion and neglects several important effects such as dispersion forces, fluctuation, hydration, ion size effects and the impact of interfacial water. Several extensions of the theory are aiming to include this in the framework of mean-field PB theory [23]. The chemical potential is simply extended by a further additive term $W_i(z)$. The interaction free energy W_i includes all other interactions of the ion with the medium and may depend on the electric potential Ψ, the concentration c_i and further parameters.

$$\mu_i = \mu_{0i} + k_B T ln(c_i) + eZ_i + W_i(z) \tag{1.9}$$

The distribution of the ion i is given by Boltzmann

$$c_i = c_{0i} \exp\left(\frac{-Z_i e\Psi(z) + W_i(z)}{k_b T}\right) \tag{1.10}$$

In the context of specific ion interactions dispersion forces become important. Ninham and Yaminsky pointed out that the van der Waals interaction is not screened by the electrolyte at the interface and may play a decisive role [25, 26]. The van der Waals attraction between the ion and the interface of the two dielectric media has a leading term as calculated by Lifschitz theory.

$$W(z) = \frac{B}{z^3} \tag{1.11}$$

This term is specific for each ion and has an inherent potential to account for specific ion effects. However, we would like to stress that several important effects cannot be captured on a mean field level such as for instance fluctuations. The sound treatment requires pair correlation functions in the general framework of statistical mechanics [27].

The explicit consideration of fluctuations can give raise to new phenomena such as a phase transition towards a condensed state of ions with increasing

surface charge. Lau et. al. predict a fluctuation driven counterion condensation [14, 15]. For a system consisting of a single charged surface and its oppositely charged counterions, Netz and Orland showed that a perturbative expansion about the mean-field PB solution breaks down if the surface charge is sufficiently high [16]. Thus, in this limit, fluctuation and correlation corrections are important and the mean-field picture must be modified [28]. To overcome this difficulty, a two-fluid model was proposed in Ref. [14], in which the counterions are divided into a free and a condensed fraction. The free counterions have the usual three-dimensional mean-field spatial distribution, while the condensed counterions are confined to move only on the charged surface and thus effectively reduce its surface charge density. The number of condensed counterions is determined self-consistently by minimizing the total free energy which includes fluctuation contributions. This theory predicts that if the surface charge density of the plate is sufficiently high, a large fraction of counterions is condensed. The result resembles features of a phase transition similar to the liquid-gas transitions. However, this theory lacks ion specific effects.

For experimentalists the situation appears as follows: The PB theory is getting more complex with a zoo of parameters accounting for the various effects which have been neglected in the original version of PB theory. There are also sound molecular dynamics simulations and several theories which go beyond the mean field level predicting new phenomena. The assessment of these theories requires reliable experimental data. The decisive information is contained in the prevailing ion distribution. Therefore experiments are required which directly assess the ion distribution.

Such an experiment is outlined in the section 2.4.4. We demonstrate that the optical reflection technique ellipsometry gives valuable insights in the prevailing ion distribution. We are able to condense the Fresnel formalism to an equation which directly relates the effective surface charge density to the measured ellipsometric signal. This equation does not contain any free parameter.

Bibliography

[1] *Current Opinion in Colloid and Interface Science*, Volume 9, Issues 1-2, Pages 1-197 (August 2004)

[2] Collins,K.D; Washabaugh,Q.; *Rev.Biophys.* **1985**, *18*, 323.

[3] P. Jungwirth and D.J. Tobias. *J Phys Chem B* 105 (2001), p. 10468.

[4] P. Jungwirth and D.J. Tobias. *J Phys Chem B* 106 (2002), p. 6361.

[5] P. Jungwirth, J.E. Curtis and D.J. Tobias. *Chem Phys Lett* 367 (2003), p. 704.

[6] D. E. Gragson, B. M. McCarty, and G. L. Richmond *J. Phys. Chem.* 1996, 100, 14272-14275.

[7] D. E. Gragson, B. M. McCarty, and G. L. Richmond *J. Am. Chem. Soc.* 1997, 119, 6144-6152.

[8] P. B. Miranda, Q. Du and Y. R. Shen *Chemical Physics Letters*, 1998, 286,1.

[9] P. B. Miranda and Y. R. Shen *J. Phys. Chem. B*, 1999, 103, 3292-3307

[10] Koelsch, P.; Motschmann, H. *Current Opinion in Colloid and Interface Science*, 9 (2004) 87-91.

[11] Koelsch, P.; Motschmann, H. *J. Phys. Chem. B* 2004, 108(48),18659-18664.

[12] Koelsch, P.; Motschmann, H. *Langmuir*, in press

[13] Manciu, M.; Ruckenstein, E *Advances in Colloid and Interface Science* **2003** , *105* 63.

[14] A.W.C. Lau, D.B. Lukatsky, P. Pincus, and S.A. Safran, Phys. Rev. E 65, 051502 (2002)

[15] A.W.C. Lau, P. Pincus, Phys. Rev. E 66, 041501 (2002)

[16] Netz, R.; Orland, H. *Eur. Phys. J. E* **2000**,*1*, 203.

[17] Moreira AG.; Netz RR. *European Physical Journal A.* **2002**, *8(1)*, 33.

[18] Jonas Örtegren, Klaus-Dieter Wantke, Hubert Motschmann and Helmuth Möhwald *Journal of Colloid and Interface Science*, 2004, 279, 266-276.

[19] A. Ben-Naim, Statistical Thermodynamics, Plenum Press, New York, **1993**.

[20] Moreira AG. Netz RR. European Physical Journal A. 8(1):33-58, (2002).

[21] Moreira AG. Netz RR. Europhysics Letters. 57(6):911-917, 2002.

[22] AG. Moreira, R.R. Netz European Physical Journal D. 21(1):83-96, 2002.

[23] D. Andelman; *Handbook of Biological Physics*, **1**, edited by R. Lipowsky and E. Sackmann (1995).

[24] O. Stern; *Z. Elektrochem.*, **30**, 508 (1924)

[25] Bostrom, D.M.R.Williams, B.W.Ninham, Phys. Rev.Lett.87 (2001) 1681.

[26] M. Bostrom, D.M.R. Williams, B.W. Ninham, Langmuir 17 (2001) 4475.

[27] R.Kjellander,S.Marcelja,J.Chem.Phys.82 (1985)2122.

[28] AG. Moreira, R.R. Netz European Physical Journal D. 21(1):83-96, 2002.

1.2 Foam stability

1.2.1 Introduction

Surfactants enable phenomena such as foaming [1]. A foam lamella consists of a thin water slab stabilized by two amphiphilic adsorption layers. Hence, it is tempting to search for correlations between the properties of the adsorption layer and the foam. This approach is in particular promising for wet foam lamellae where both adsorption layers are separated by a fairly thick water slab. Different rules may apply for Newton black films, where the adsorption layers are so close that their interaction governs the system behavior. An excellent review for these system is given in the book of Exerowa et. al.[2].

All foams are thermodynamically unstable, due to their high interfacial energy, which decreases upon rupture. The stability of foams has been classified into two extreme types, the unstable or transient foams with lifetimes of seconds and the meta-stable foams with lifetimes of several minutes to hours. Champagne and beer foam are classical examples for both extremes. In the context of foams, it is desirable to distinguish between foam formation and foam stability. Foam formation could successfully be linked to the dynamic surface pressure [3], however, so far it turned out to be impossible to relate foam stability to a fundamental system parameter of the adsorption layer.

For a system of such a complexity it is not too surprising that an uniform theory for the mechanism of foam stability has not yet been developed. A real foam is a complicated three dimensional network of connected foam lamellae which are all subject to complex drainage and flow processes. However, it is obvious that the response of the system to a mechanical disturbance or thermal thickness variations is of utmost importance. These processes disturb the adsorption equilibrium and as a consequence surfactants have to be transported via a Marangoni flow or via the coupled bulk phase to the interface to restore the equilibrium coverage. It is the aim of the present study to correlate the stability of an individual foam lamella with the surface dilational rheology of its constituent adsorption layer. For this purpose we produce foam lamellae from a highly purified surfactant solution by a defined protocol and correlate their lifetime with the real and imaginary part of the surface dilational modulus E. In the following section the key concepts of surface rheology are reviewed.

1.2.2 Surface rheology

The adsorption changes the surface tension. The difference between the surface tension of film covered γ_{film} and the bare water surface $\gamma_{\text{H}_2\text{O}}$ can be interpreted as a surface pressure Π (physical units [N/m])

$$\Pi = \gamma_{\text{H}_2 0} - \gamma_{\text{film}} \tag{1.12}$$

Soluble surfactants adsorb at the interface and are in equilibrium with the bulk. Gibbs equation states that the surface excess Γ [g/m^2] is proportional to the derivative of the equilibrium surface tension isotherm with respect to the logarithm of the bulk concentration c.

$$\Gamma \propto \frac{\partial \gamma_e}{\partial \ln c} \tag{1.13}$$

The surface elastic modulus E is defined in analogy to the corresponding bulk quantity as the change in the surface pressure Π upon a relative area change $\delta A/A$. Basically, it is a measure for the ability of the system to adjust its surface tension in an instant of stress.

$$E = -A\frac{\partial \Pi}{\partial A} = -\Gamma \frac{\partial \Pi}{\partial \Gamma} \tag{1.14}$$

The latter relation holds since the surface excess Γ is proportional to the inverse of the area per molecule. The surface dilational viscosity κ can be introduced as the imaginary part of the complex module E that describes the linear response to a sinusoidal deformation of the frequency ω.

$$E(\omega, c) = |E(\omega, c)| \exp(i\phi(\omega, c)) = \epsilon(\omega, \Gamma) + i\kappa\omega \tag{1.15}$$

where the real part $\epsilon(\omega, \Gamma)$ is the storage modulus that depends on the surface composition and the frequency. The experimental determination of the dilational parameters ϵ and κ require the measurement of the dynamic surface tension upon harmonic compression and expansion cycles of the surface layer. The relative area change $\delta A/A$ and the surface tension γ_e yields the surface dilational modulus E. Several arrangements have been used and proposed, the classical experiment uses oscillating moving barrier devices

producing harmonic surface area changes of a monolayer. For technical reasons theses methods are restricted to the subfrequency region [5]. During a compression or expansion process, the concentration of monolayer molecules is higher or lower in the vicinity of the barrier, respectively, than far from it. Hence a surface pressure gradient is created which induces a surface flow, the so-called Marangoni flow [6] which overlaps with relaxation processes in the monolayer. Furthermore the movement of the barrier induces longitudinal waves which can be periodically reflected at the barriers if the wavelength is on the order of the trough length. This results in a superposition of different waves in the film which makes the determination of the dilational parameters ϵ and κ rather difficult. In a theoretical approach, Lucassen and Barnes [7] stated that the length of the longitudinal wave λ must be 8 times higher than the length L of the trough ($\lambda \geq 8L$) to avoid this effect.

A bigger frequency range can be covered by the excitation of surface waves and their optical evaluation [8, 9]. A further common alternative is oscillating drop/bubble shape tensiometry. The shape of a drop is given by the balance between gravity and surface tension. The evaluation of the drop shape according to the Gauss-Laplace equation yields the surface tension and the corresponding surface area. The Gauss-Laplace equation has been derived for static conditions, an oscillation causes deviation from the ideal shape. In order to estimate the limiting frequency, dynamic measurements of surfactant-free systems were done where both the elasticity and viscosity should be zero. Any positive or negative values for the elasticity or viscosity would then refer to artefacts caused by a deformation rate larger than a critical value. A recent study [10] shows that dynamic drop and bubble shapes can only be well described by the GaussLaplace equation for oscillations with frequencies up to 1Hz if the viscosity is $\eta = 1cP$ (water, ethanol). A much lower critical frequency of about 0.1 Hz is obtained for drops of a very viscous silicon oil ($\eta = 1000cP$). Thus, the shape analysis tensiometry is applicable for dilational rheology studies up to a frequency of 1 Hz as maximum. This holds true for drops and bubbles. For higher frequencies alternative methods have to be applied in order to measure the elasticity and viscosity of interfacial layers. This limit has to be kept in mind especially since the technical parameters of some commercial instruments allow much faster oscillation (up to 40 Hz).

1.2.3 The oscillating bubble

An interesting and superior alternative is capillary pressure tensiometry [11]. Instead of analyzing the drop shape, the pressure difference p_c across a bubble interface is analyzed using the Young-Laplace equation. The pressure $p_c(t)$ is measured by a pressure transducer and the drop radius r is calculated by the volume displaced by the piezo translator. The dynamic interfacial tension $\gamma(t)$ is then given:

$$\gamma(t) = \frac{p_c(t)r(t)}{2} \tag{1.16}$$

We describe in chapter 2.5 a variant of this concept that allows the measurement of the complex surface dilation modulus of aqueous surfactant solutions in a frequency range of 1-to 500 Hz. This extension in frequency of about two decades compared to the shape analysis tensiometry can be obtained by a special treatment of a capillary where the air bubble is formed and the direct measurement of the pressure within the liquid using a piezo transducer instead of a shape analysis. Due to a harmonic expansion and compression of the interface the technique of an oscillating bubble suppresses unwanted features as Marangoni flow and bulk contributions can be separated by calibration measurements.

The extension of the frequency range is crucial for the investigation of soluble surfactants. If adsorption layer and bulk are in thermodynamic equilibrium, the surface coverage is determined by the bulk concentration c. The equilibrium is disturbed upon compression or expansion, and as a consequence amphiphile must dissolve to the bulk phase or adsorb at the interface to restore the equilibrium coverage. Let's consider two limiting cases: The frequency of the oscillation is much slower than the molecular exchange process so that the mono-layer remains in equilibrium at all times. As a consequence, there is no resistance to the compression or expansion and E vanishes. If the frequency of the oscillation is much higher than the molecular exchange processes, the mono-layer is decoupled from the bulk and behaves similar to an Langmuir layer of an insoluble amphiphile as described by eqn. 1.14.

The dependence in the intermediate frequency range has been first described by Lucassen et al. [12]:

$$E = \epsilon_o \frac{1+\Omega}{1+2\Omega+2\Omega^2} \quad (1.17)$$

$$\omega\kappa = \epsilon_o \frac{\Omega}{1+2\Omega+2\Omega^2} \quad (1.18)$$

with $\Omega = \sqrt{(D/2\omega)}dc/d\Gamma$ and D being the diffusion coefficient of the surfactant in the bulk. The Lucassen model has been extended to account for further observational facts. [13, 14]. The situation is plotted in Figure 1.4 for typical values of the diffusion coefficient and $dc/d\Gamma$. Obviously it is of utmost importance that the oscillation occurs in the right time window. For classical soluble surfactants, the most interesting frequency range is 1 to 500 Hz which is covered by our device as described in section 2.5.

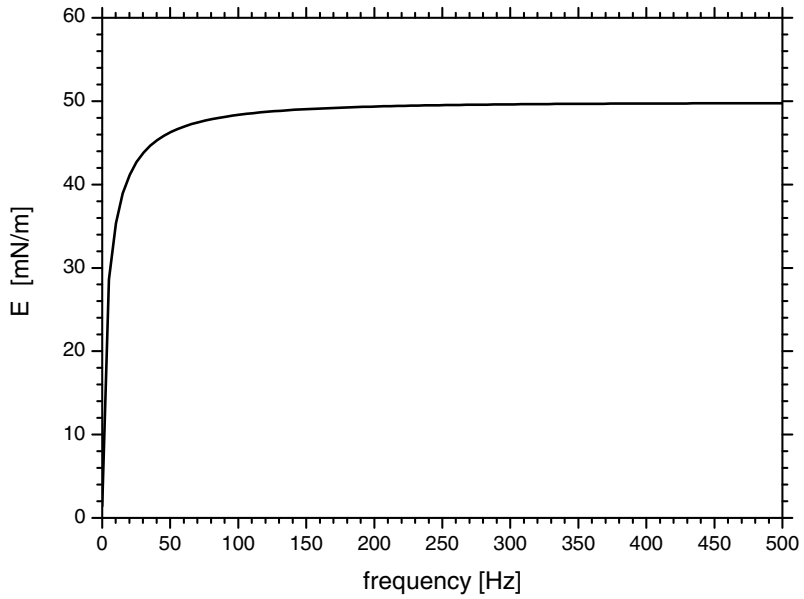

Figure 1.4: Magnitude of the complex modulus E as a function of the frequency ω of oscillation as described by the Lucassen et al. Typical values for surfactants were used for the calculations: $D = 5 * 10^{-5} cm^2/s$, $dc/d\Gamma = 200 cm^{-1}$ and $\epsilon_0 = 50 mN/m$.

Bibliography

[1] R.J. Pugh,
Foams and Foaming
Handbook of Applied Colloid and Surface Chemistry,
edited by Krister Holmberg, John Wiley&sons (2001).

[2] D. Exerowa, P. Kruglayakov, Foams and Foam films, Studies in Interface Science Elsevier, New York, Oxford (1998).

[3] Engels, Th., von Rybinski, W., Schmiedel, P., Progr. Coll. Polym. Sci., **111**, 117, (1998)

[4] K.-D. Wantke, H. Fruhner, in: D. Möbius, R. Miller (Eds.), Studies in Interface Science, vol. 6, Elsevier, Amsterdam, (1998), p. 327.

[5] G. Kretschmar, J. Li, R. Miller, H. Motschmann *Colloids and Surfaces A*, **114**, 227, (1996).

[6] D.S. Dimitrov, I. Panaiotov, P. Richmond and L Ter-Minassian-Saraga, *J. Colloid Interface Sci.*, 65 (1978) 483.

[7] J. Lucassen and G.T. Barnes, J. Chem. Soc., *Faraday Trans. 1*, 68 (1972) 2129.

[8] D. Langevin, Ed. , Light Scattering by Liquid Surfaces, chapter 11, M. Dekker, 1992.

[9] A. Bonfillon, D. Langevin, Langmuir **9**, 2172, 1993,

[10] M.E. Leser, S. Acquistapache, A. Cagna, A.V. Makievski, R. Miller Colloids and Surfaces A: Phsicochem. Eng. Aspects, (in press)

[11] L. Liggieri, V. Attolini, M. Ferrari, and F. Ravera Journal of Colloid and Interface Science **255**, 225, (2002).

[12] E.H. Lucassen, J. Lucassen, Adv. Colloid Interface Sci. **2**, 347, (1969).

[13] J. Lucassen, R. Hansen, J. Colloid Interface Sci. **23**, 319 (1967).

[14] J. Lucassen, M. van den Tempel, M., J. Colloid Interface Sci. 41, 491

Chapter 2

Experimental section

2.1 Materials

The choice of a model system is crucial. As a surfactant we used 1-dodecyl-4-dimethylaminopyridinium bromide (C12-DMPB):

Figure 2.1: Chemical structures of the cationic amphiphile 1-dodecyl-4-dimethylaminopyridinium bromide, C12-DMPB

The surfactant resemble the following features:

- It is a classical ionic surfactant.
- It possess a critical micelle concentration (cmc).
- It is a strong electrolyte following the prediction of the Debye-Hückel theory.

- The headgroup is a push pull π system that provides a sufficiently high hyperpolarizibility to fully utilize the potential of surface second harmonic generation (SHG), which monitors the number density and the orientation of the headgroup only. All other elements do not contribute to the SHG signal.

2.2 Sample preparation

Due to the peculiarities of surfactant synthesis, many surfactants contain trace impurities of higher surface activity than the main component. These trace impurities do not influence bulk properties. However, at the surface they are enriched and impurities may even dominate the properties of the interface. This behavior was first recognized by Mysels [2] and a purification scheme using foam fractionation was proposed [3]. A detailed discussion on artifacts caused by impurities can be found in [4].

In studies performed in our lab, we use a fully automated purification device developed by Lunkenheimer et. al. which ensures a complete removal of these unwanted trace impurities [5]. The aqueous stock solution undergoes numerous purification cycles consisting of a) compression of the surface layer, b) its removal with the aid of a capillary, c) dilation to an increased surface and d) formation of a new adsorption layer. At the end of each cycle the surface tension γ_e is measured. The solution is referred to as surface chemically pure grade if γ_e remains constant in between subsequent cycles. Quite frequently more than 300 cycles and a total time of several days are required to achieve the desired state. The sample preparation is time consuming and tedious but mandatory for the investigation of equilibrium properties of adsorption layers of soluble surfactants at the air-liquid interface.

Solutions of different concentrations were prepared by diluting the stock solution. The surface tension measurements where repeated after several months with the same stock solution and no measurable change in the equilibrium surface tension isotherm could be detected. In addition, time dependent measurements of the surface tension at distinct concentrations have been performed. The surface tension was immediately stable at all concentrations.

2.3 Nonlinear optics

The experimental investigation of monolayers of soluble surfactants faces the following difficulties.

- The number density of the surfactants is low requiring a submonolayer resolution
- The bulk phase contains dissolved amphiphiles requiring discrimination between adsorbed and dissolved species

The nonlinear optical techniques of second harmonic generation (SHG) and infrared-visible sum frequency generation (IR-VIS SFG) satisfy all these requirements. Using laser sources, they share all of the advantages of optical techniques. The key feature is the inherent surface specificity. The gas or bulk phase with its random distribution of molecules does not contribute to the spectra. This fact makes SHG and IR-VIS SFG a powerful tool for the investigation of aqueous and solid interfaces. Their sensitivity to submonolayer coverages of adsorbates has been demonstrated in many experiments.

In IR-VIS SFG studies, a pulsed tuneable infrared laser beam and a visible beam are mixed at an interface to produce a SFG signal. Surface active vibrational modes of molecules at the interface result in a resonant enhancement of the SFG response, thus spectroscopic information about the molecules can be obtained. Only molecules at the interface are SFG active. The SFG signal contains information about molecular orientation and arrangement. By using different combinations of polarization for the pump beams important features about the distribution of the adsorbate orientation can be deduced. Due to the difficult handling of an IR-VIS SFG setup, its used only by a handful of investigators around the world, but the use is growing as more investigators discover the unique information that can be gained from its applicability to a wide range of systems.

Since IR-VIS SFG detects vibrational modes, which are rather localized to specific groups of atoms within the molecules, the relative orientation of different groups within the same molecule can be obtained. Phase measurements provide information about the absolute orientation of molecules with respect to the surface.

SHG is closely related to IR-VIS SFG. The mixing process occurs between two photons of the same energy. Simply speaking IR-VIS SFG can be regarded as a surface specific infrared spectroscopy of the surface layer. Second harmonic generation can be regarded as a surface specific UV-VIS spectroscopy.

2.3.1 Vibrational infrared-visible sum frequency generation IR-VIS SFG

Figure 2.2 provides an illustration of an IR-VIS SFG experiment for the air/water interface. Light pulses from a visible laser ω_{vis} and a tunable IR-laser ω_{IR} are coincident in time and space at the interface. The electric fields of the incident radiation induce a non-linear polarization at the sum frequency of the two incident beams which is the source term for coherent radiation $\omega_{\text{vis}} + \omega_{\text{IR}}$ in a well defined direction. When the infrared source is tuned through the spectral region of interest, coincidence between the photon energy and the energy of the molecular vibrational mode results in a resonant enhancement of the SFG response.

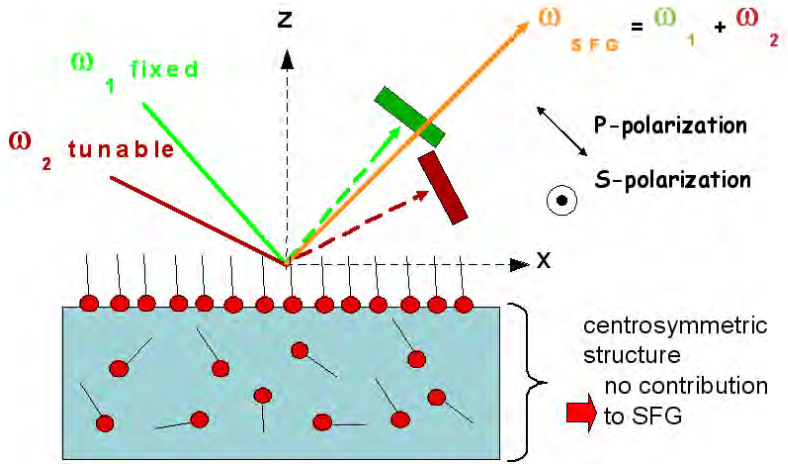

Figure 2.2: Schematic of the IR-VIS SFG method as applied to air/water interfaces. P and S correspond to the polarization of the light either parallel or perpendicular to the incident plane, respectively.

The surface specificity is a direct consequence of a second-order non-linear

optical process. A symmetry consideration reveals that in dipole approximations all χ^2 processes are forbidden in media with inversion symmetry. At the interface of two isotropic phases the inversion symmetry is broken and consequently an IR-VIS SFG signal is produced within the interfacial region. [6, 7]. This inherent surface sensitivity makes it an advantageous method of studying the vibrational spectroscopy of molecules at surfaces as compared to linear vibrational spectroscopies such as infrared or Raman spectroscopy. The disadvantage is the complex handling and the difficulty in measuring IR-VIS SFG spectra over a broad IR frequency range (due to limitations in IR laser systems used) and the weak SFG signals due to the higher order nature of the response.

2.3.2 Theory of IR-VIS SFG

Second order nonlinear optical processes are forbidden in a medium with inversion symmetry, which is necessarily broken at an interface, where the nonlinear processes are therefore allowed. The incident infrared and visible light beams are inducing dipole oscillations in the medium. For a driven anharmonic oscillator, the induced dipole moment $p(\omega_{\mathrm{vis}}+\omega_{\mathrm{ir}})$ is proportional to the quantity $E(\omega_{\mathrm{vis}})E(\omega_{\mathrm{ir}})$, the product of the incoming fields of strengths $E(\omega_{\mathrm{vis}})$ and $E(\omega_{\mathrm{ir}})$. The induced sum frequency dipole per unit volume, the polarization $P^{(2)}(\omega_{\mathrm{vis}}, \omega_{\mathrm{ir}})$, can be written as

$$P^{(2)}(\omega_{\mathrm{sfg}}) = \chi^{(2)}(-\omega_{\mathrm{sfg}}, \omega_{\mathrm{vis}}, \omega_{\mathrm{ir}})E(\omega_{\mathrm{ir}})E(\omega_{\mathrm{vis}}) \tag{2.1}$$

where $\chi^{(2)}$ is known as the nonlinear susceptibility and is a characteristic coefficient of the medium. The microscopic expression for $\chi^{(2)}$ can be obtained from second order perturbation theory. For the case of only one frequency ω_{ir} on resonance, $\chi^{(2)}$ can be written as $\chi^{(2)} = \chi^{(2)}_{NR} + \chi^{(2)}_{R}$, the sum of the nonresonant and resonant part respectively of $\chi^{(2)}$. The resonant term, $\chi^{(2)}_{R\nu}$ is dependent on the number of molecules N and the orientationally averaged molecular hyperpolarizability $< \beta_\nu >$ of the $\nu - th$ vibrational mode in the following way:

$$\chi^{(2)}_{R\nu} = \frac{N}{\epsilon_0} < \beta_\nu > \tag{2.2}$$

Given the expressions in eqs 2.1 and 2.2, the square root of the sum frequency intensity is shown to depend on the number of molecules giving rise to the response ($I_{SFG} \propto |P_{SFG}|^2$). Their average orientation can be derived through the $< \beta_\nu >$ term. These two contributions can be used to determine the orientation of interfacial molecules and changes in orientation under various experimental conditions as it is shown in 2.3.8.

The enhancement in the sum frequency response that occurs when the frequency of IR radiation is resonant with a sum frequency active vibration arises from the molecular hyperpolarizability, $< \beta_\nu >$. This enhancement in the molecular polarizability is given by

$$\chi^{(2)}_{R\nu} \propto \frac{A_K M_{IJ}}{\omega_\nu - \omega_{ir} - i\Gamma_\nu} \tag{2.3}$$

In this expression A_K is the IR transition moment, M_{IJ} is the Raman transition probability, ω_ν is the resonant frequency and Γ_ν determines is the line width of the transition. Thus, a transition must be both optically Raman and infrared active in order to be detected by SFG. This is consistent with the requirement from macroscopic symmetry considerations that there must be a lack of inversion symmetry in the medium for $\chi^{(2)}_{R\nu}$ to be nonzero.

2.3.3 IR-VIS SFG setup

In order to obtain tunable infrared laser pulses an optical parametric generator (OPG) was pumped by a Continuum PY61-series pump laser. The visible light beam was obtained by frequency doubling of the 1064 nm beam of the pump laser in a KTP crystal using type II phase matching. In the following sections the pump laser, the laser bench, the OPG and the sample stage are illustrated.

2.3.4 The pump laser

As a pump laser a Continuum PY61 laser producing high energy ($\sim$ 30 μJ), short duration pulses ($\sim$ 35 ps FWHM) at a rate of 10 Hz from Nd:YAG lasing media was used. The lasing wavelength was 1064 nm.

Figure 2.3 shows the arrangement of the laser bench. In order to achieve

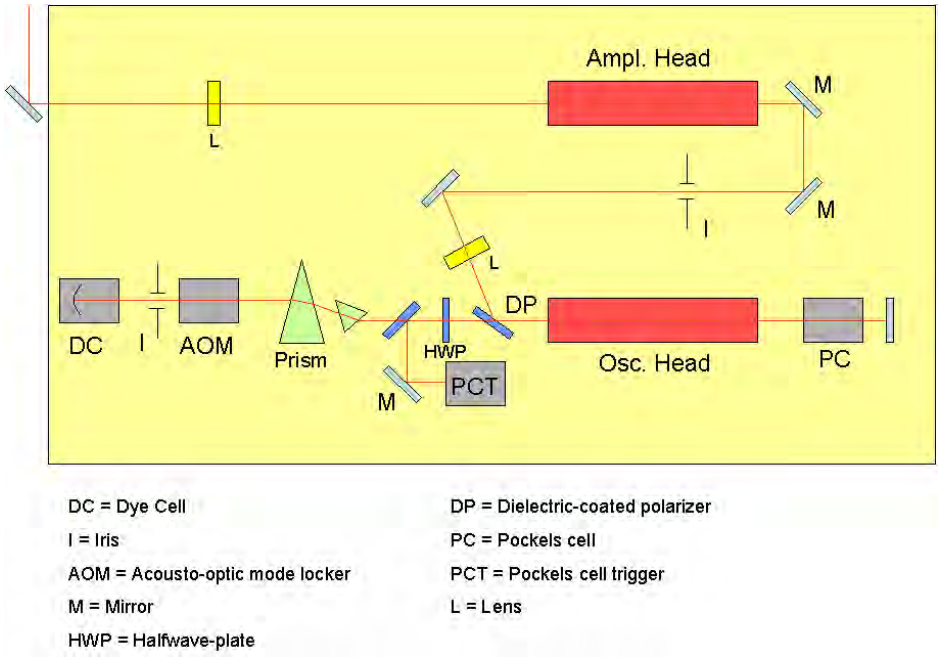

Figure 2.3: Continuum PY61 pump laser

high-energy single pulses, a two-stage amplification process was used. Population inversion in the Nd:YAG lasing media was accomplished by optically pumping a cylindrical Nd:YAG rod with two high-brightness linear flashlamps. The optical pumping efficiency is maximized by placing both the rod and the flashlamps inside a head whose interior is a highly reflecting magnesium oxide diffuser. The high pumping efficiency minimizes thermal loading of the rods in the head (although the head must still be water-cooled). In the first stage, a relatively low energy pulse is obtained in the oscillator cavity, which is both actively and passively mode-locked. Active mode-locking is accomplished by an acousto-optic mode locker that modulates the cavity loss by creating an ultrasonic sound wave-generated diffraction grating in the oscillator cavity. Passive mode-locking is accomplished by a saturable absorber dye (Q-Switch # 1) dissolved in 1,2-dichloroethane circulated through a dye cell on which the longitudinally oscillating electromagnetic modes are incident. The saturable absorber modulates the cavity loss at the mode separation frequency. This active-passive modelocking scheme results in greater stability in the pulse energy and a smaller number of missed shots.

The mode-locking scheme results in a train of pulses separated by a time $T = 2\pi/\Delta$, where $\Delta = \pi c/L$ is the mode separation frequency, and L is the cavity length. In order to obtain a high energy amplified pulse, a pulse slicer is used to select the highest energy pulse from the pulse train in the oscillator and dump it out of the cavity. The pulse slicer consists of a photodiode that monitors the intensity buildup in the oscillator cavity connected to a Marx board-driven Pockels cell that can be quickly switched on. Shortly before the maximum intensity pulse, the Pockels cell is switched on resulting in a 90° rotation of the polarization of the field inside the cavity during the time in which the Pockels cell is on. The resulting polarized pulse is reflected out of the oscillator cavity by a dielectric-coated polarizer (DP). This cavity dumping method of pulse extraction results in a higher energy extracted pulse, because nearly the entire energy of the pulse is removed from the oscillator cavity, rather than the small percentage that usually makes it through a typical oscillator cavity, where one of the end mirrors is slightly transmitting at the lasing wavelength. The spatial profile of the sliced pulse is then optimized by focussing on a pinhole and steered afterwards through the flashlamp-pumped population inversion in the amplifying rod. This results in a large stimulated emission from the amplifying rod, since the oscillator pulse contains very many photons having the same frequency as the laser transition. There is typically a factor of 9-12 times energy amplification of the input pulse (from $\sim$ 5 μJ to $\sim$ 45 - 60 μJ).

2.3.5 The laser bench

The amplified output 1064 nm beam of the Continuum PY61 laser pump is then split to produce a visible pulse of 20 μJ at 532 nm by frequency doubling in a KTP crystal using type II phase matching (SHG in Figure 2.5). Afterwards the 532 nm beam is split into three portions: One beam is entering directly the OPG (H1), one is passing through a dove prism on a sliding stage and is entering the OPG afterwards (H2) and one beam is going through a delay line (dove prism on a sliding stage) passing through a $\lambda/2-$ plate (HW) and a polarizer for attenuation and through a $\lambda/2-$ plate on a rotary stage to adjust the polarization before the SFG sample stage. The 1064 nm pulse is entering directly the OPG (H3).

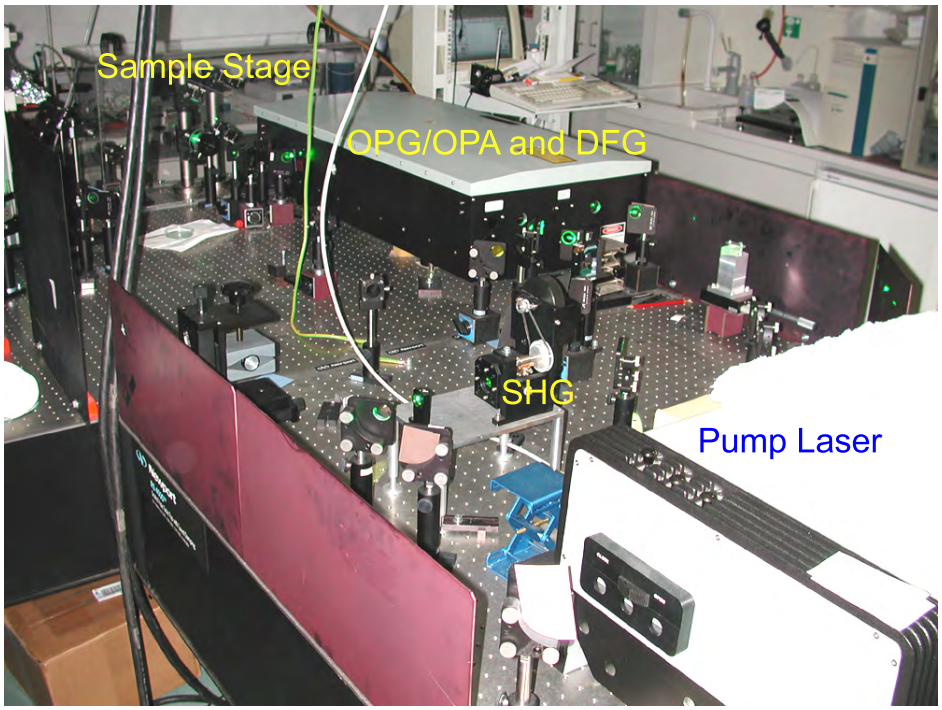

Figure 2.4: Laser bench

2.3.6 Generating tunable infrared light

The OPG stage employs optical parametric generation, optical parametric amplification and difference frequency mixing to convert Nd:YAG pump laser radiation into mid-infrared light continuously tunable from 2.8 to 4 μm. These nonlinear three-wave mixing processes are closely related to harmonic generation where two photons at a longer wavelength are converted to one photon at a shorter wavelength through the nonlinear interaction with a suitable material. Like other coherent interactions, the conditions for energy and momentum conservation must be met in order for the process to occur.

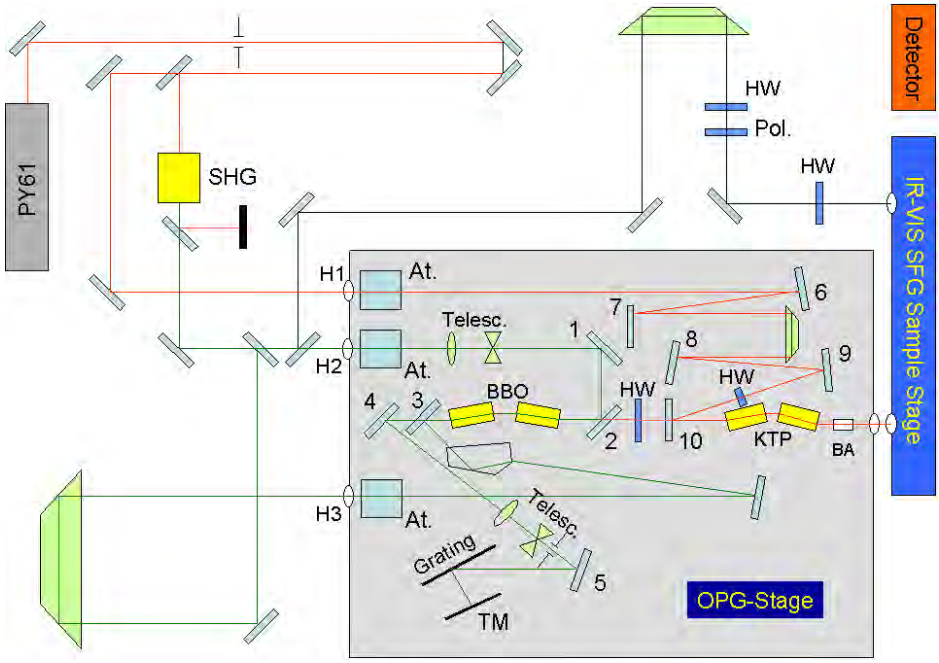

Figure 2.5: Laser bench and OPG

Figure 2.6: OPG/OPA stage and DFG

Given a material with suitable nonlinear and transmission properties such as beta barium borate (BBO) optical parametric oscillation or amplification may occur when the frequencies of the three photons conserve energy, $\omega_p = \omega_s + \omega_i$, and the wave vectors of the three photons conserve momentum, $k_p = k_s + k_i$. In the parametric process, these three photons are commonly referred to as the pump, signal and idler, corresponding to the highest, intermediate and lowest photon energy.

The most common method to achieve the simultaneous conservation of energy and momentum takes advantage of the birefringence of certain materials. The materials have two indices of refraction for the two different polarizations of light and one index changes with changes in propagation direction through the crystal. It is possible to choose a combination of polarization and angles that allow energy and momentum to be conserved for a given combination of wavelengths. Changing the angle of the crystal changes the wavelength for which energy and momentum are conserved. The angle tuning of birefringent materials so that both energy and momentum are conserved, is called angle phase matching. Phase matching is required for efficient optical parametric generation.

The OPG is designed to produce picosecond, narrow-band radiation with wavelengths ranging from 2.8 to 4 μm and is pumped by the Continuum PY61 pump laser. To generate tunable infrared light four basic steps are necessary:

1. The optical parametric generation of broadband signal radiation from 725 to 900 nm (OPG). This is done by passing the second harmonic 532 nm beam (the pump wavelength) through BBO crystals. The idler produced by this step is not used.

2. The bandwidth narrowing of the broadband signal by a diffraction grating and the wavelength selection by a tuning mirror.

3. The amplification of the narrow-bandwidth signal by fresh second harmonic 532 nm beam in a second pass through the BBO to produce an idler output from 1.3-2,0 μm (OPA). Steps 1-3 are collectively referred to as OPG/OPA.

4. Mixing the idler of the OPG/OPA stage with the fundamental of the

Nd:YAG laser (1064 nm) in a KTP crystal to produce 2,8-4,0 μm radiation.

The layout of the OPG is shown in Fig 2.5. The fundamental 1064 nm beam is entering through hole H1. The first second harmonic 532 nm beam of the Nd:YAG pump laser enters through hole H2 whereas the second 532 nm beam is entering after passing through a dove prism on a sliding stage in hole H3.

The 532 nm beam through hole H2 is attenuated to 3.5 μJ and then down telescoped to approximately 2 mm and left rather divergent, for reasons explained below. It is then turned 180 degrees by mirrors 1 and 2. The first pass through the BBO crystals produces the OPG. The BBO crystals are rotated so that the broad band radiation is centered on the desired wavelength.

After the OPG the broad band signal is transmitted through dichroic mirror 3. Mirrors 4 and 5 then steer it to the grating. The first order reflection off the grating goes to the tuning mirror, which is positioned so that the desired wavelength will be autocollimated (using another first order reflection off the grating).

In order to maintain calibration of the output wavelength, it is necessary to keep the angle of incidence on the grating consistent. Therefore an iris is included. If the beam is directed through the center of the iris by mirror 4, the wavelength will match the one once calibrated.

The telescope before the grating served mainly to collimate the very divergent signal beam. It is an up (expanding) telescope on the way to the grating and a down telescope on the way back. The expansion of the beam going to the grating also helps to illuminate more lines on the grating, and therefore narrow the bandwidth - even though this effect is minimal.

The narrow bandwidth signal beam returning from the grating is then mixed with properly delayed 532 nm beam entering through hole H3 and attenuated to 3.5 μJ. The use of a 'fresh' 532 nm beam for the amplification of the signal beam was implemented in order to ensure properly amplification of the signal beam in the second pass through the crystals. This is the OPA stage. The BBO crystals are 20 cm apart to prevent them from broadening the bandwidth. It is very desirable that little or no broad band OPG take place on the second OPA pass of the 532 nm beam through the BBO crystals.

Therefore the 532 nm beam is divergent, so that it is nearly twice as large for the OPA pass and therefore the intensity is below the OPG threshold.

The idler of the OPG/OPA stages then passes through dichroic mirror 2, a $\lambda/2-$plate and a 1064 nm reflector (10) to the KTP crystals where it is being mixed with the properly delayed 1064 nm beam originated from hole H1. The resulting beam will be 2.8 - 4.0 μm. The 1064 nm beam has been reflected by mirrors 6-10, as well as the dove prism. The dove prism is mounted on a sliding stage and is used to adjust the delay for the best temporal overlap with OPG/OPA idler beam. The compensating crystal prevents beam walk-off as the mixing crystal is angle tuned.

The 1064 nm and the idler of the OPG/OPA stage is filtered by a brewster angle plate (BA) on a rotary stage, so that only the desired wavelength (2.8 - 4.0 μm) is entering the SFG sample stage.

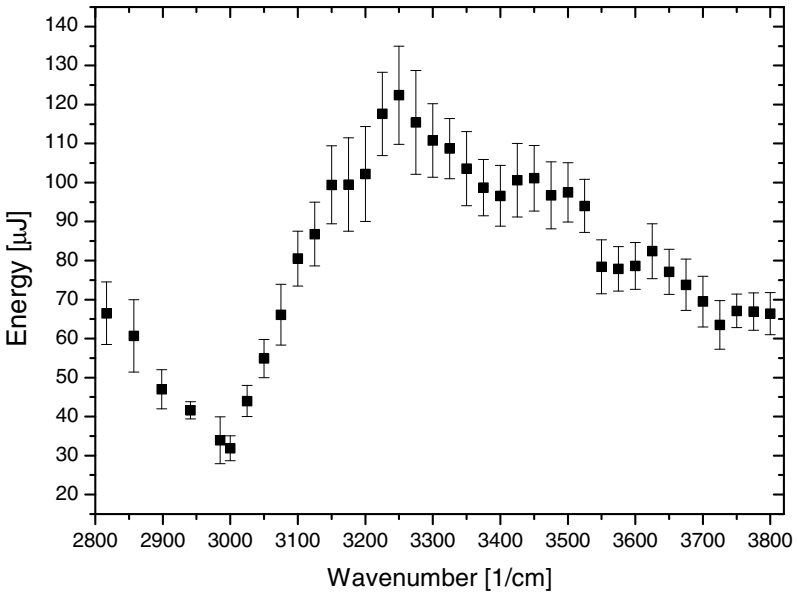

Figure 2.7: OPG output Energy as a function of the wavenumber

In Figure 2.7 the OPG output intensity as a function of the wavelength is plotted. The intensity was measured by a photodiode. All spectra were

normalized by this energy curve.

2.3.7 SFG sample stage

The sample stage contains the mixing of infrared and visible light beams at the sample and the detection of the sum frequency generated signal with a photomultiplier (Figure 2.8). The sample stage is covered by a plastic box which is purged with nitrogen in order to prevent adsorption of infrared light before the sample. The polarization of the visible light can be tuned by a $\lambda/2$ plate in a rotary stage (HW). The polarization of the infrared light beam can be changed from $\hat{p}$ to $\hat{s}-$light by changing the arrangement of mirrors. The angle of incidence for visible and infrared light beam were 55° and 62°, respectively.

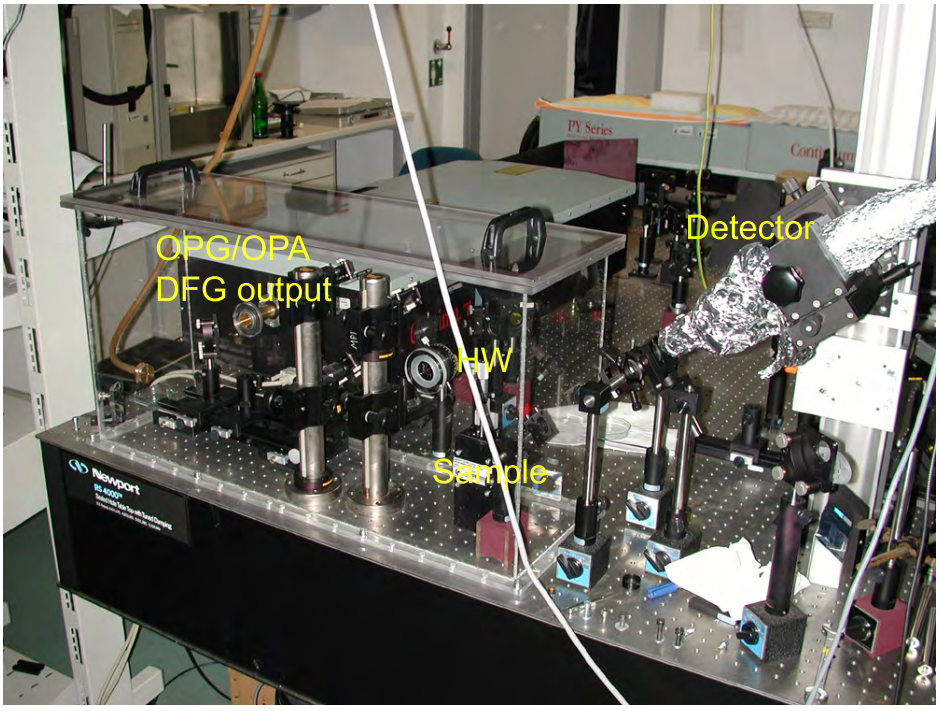

Figure 2.8: SFG sample stage and detector

The sum frequency generated light is collected by a lens. A holographic notch filter and several bandpass filters preventing the passage of light other

then the SFG light. The SFG light is then detected by a Burle photomultiplier (ME30FK).

The photon fluxes from the SFG experiment for each laser shot were converted into electrical currents by the photomultiplier tube. These pulses were digitized by an oscilloscope (HP54520, 2-GSa/sec.) which was triggered by a photodiode placed at the output of the pump laser. For each shot the integral of the signal versus time curve in the oscilloscope was taken as the photon intensity of the SFG light. Usually for each wavelength about 300 shots were taken. The oscilloscope was connected to a computer which automatically evaluate the data from the oscilloscope and triggers a new wavelength for the OPG.

2.3.8 Second harmonic generation (SHG)

SHG is a nonlinear optical second order $\chi^{(2)}$ process, the generation of frequency doubled light is the result of the interaction of a high power laser pulse with matter. It has been used for decades to extend the frequency range of laser light sources using non-centrosymmetric crystals. SHG as a surface specific tool exploits the fact that there is no generation of SHG light in centro-symmetric media. At the interface of two isotropic media the centrosymmetry is broken and SHG light is generated within the transition region of both adjacent media [6, 8].

In favorable cases, the analysis of polarization dependent SHG measurements allows the determination of the symmetry of the interface, the number density N of the amphiphiles within the topmost layer and the orientation of the molecules in the interfacial layer. Depending on the hyperpolarizability β of the adsorbed molecules, a submonolayer sensitivity of about 1/100 of a monolayer can be achieved [9, 10].

Unfortunately, only certain molecules give rise to a SHG signal and in order to fully exploit the potential offered by SHG it is necessary to design a suitable model system with a high hyperpolarizability. The SHG signal is then determined by the dipole contribution and measures the components of the macroscopic susceptibility tensor $\chi^{(2)}$ which is related to the molecular quantities by the oriented gas model [11]:

$$\chi^{(2)} = \sum_{\text{mol}} \beta = N\langle\beta\rangle \tag{2.4}$$

It states that the susceptibility $\chi^{(2)}$ is the sum of the hyperpolarizabilities β of all molecules. This can also be expressed in terms of their number density, N, and their corresponding orientational average $\langle\beta\rangle$ as denoted by the brackets. Therefore the square root of the SHG frequency intensity ($I_{SHG} \propto |P_{SFG}|^2$) is shown to depend on the number of molecules giving rise to the response and their average orientation which can be derived through the $\langle\beta\rangle$ term.

The macroscopic susceptibility tensor $\chi^{(2)}$ is defined in the laboratory frame of reference (I, J, K) as given by the plane of incidence, the hyperpolarizability β is defined in the molecular frame of reference (i, j, k). Both third rank tensors can be transformed using an Euler transformation [12]

$$\beta_{IJK} = \mathbf{U}_{Ii}(\phi,\theta,\psi)\beta_{ijk}\mathbf{U}^{-1}_{Jj}(\phi,\theta,\psi)\mathbf{U}^{-1}_{Kk}(\phi,\theta,\psi) \tag{2.5}$$

with $\mathbf{U} = \mathbf{R_c}\mathbf{R_b}\mathbf{R_a}$ and the $\mathbf{R_i}$ are describing the subsequent rotation around three axis a, b, c.

$$R_c(\psi) = \begin{pmatrix} \cos\psi & \sin\psi & 0 \\ -\sin\psi & \cos\psi & 0 \\ 0 & 0 & 1 \end{pmatrix}, \; R_b(\phi) = \begin{pmatrix} \cos\phi & \sin\phi & 0 \\ -\sin\phi & \cos\phi & 0 \\ 0 & 0 & 1 \end{pmatrix}$$

$$R_a(\theta) = \begin{pmatrix} \cos\theta & 0 & -\sin\theta \\ 0 & 1 & 0 \\ \sin\theta & 0 & \cos\theta \end{pmatrix} \tag{2.6}$$

$$\tag{2.7}$$

Evaluation of this equation is a tedious procedure involving lengthy expressions relating the individual tensor components. The explicit calculation can be found in [13] or can be conveniently generated with the aid of algebraic computer math packages (e.g. Mathematica, Wolfram Research).

From our experimental arrangement these equations are significantly simplified. The chromophore used in this study is dominated by its β_{zzz} component with its value being orders of magnitude greater than any other el-

ement of the tensor. Thus the β-tensor can be treated as a scalar quantity. In addition the number of independent tensor elements is further reduced by the symmetry in the arrangement of the molecules. In our experiment a $C_{\infty v}$-symmetry with an isotropic azimutal distribution of the molecules is observed. The remaining tensor elements are

$$\begin{aligned} \chi_{zzz} &= N\beta_{zzz}\langle\cos^3\theta\rangle \\ \chi_{xxz} &= \chi_{xzx} = \chi_{zxx} = \chi_{yyz} = \chi_{zyy} = 1/2N\beta_{zzz}\langle\cos\theta\sin^2\theta\rangle \end{aligned} \quad (2.8)$$

Thus an SHG -analysis allows the determination of the number density and the orientation of the chromophore.

The most accurate determination of the tilt angle can be achieved by a continuos rotation of the plane of polarization P of the incident beam at fixed settings of the analyzer A. With the aid of Maxwell's equations a relation between the intensity $I^{2\omega}$ and I^{ω} can be derived. For an analyzer setting at $\hat{p}$ the following equation holds

$$I^{2\omega} = D|(A\cos^2 P + C\sin^2 P)\chi^{(2)}_{zxx} + B\cos^2 P\chi^{(2)}_{zzz}|^2 I(\omega)^2 \quad (2.9)$$

with

$$\begin{aligned} A &= (F_z(2\omega)F_x(\omega) - 2F_x(2\omega)F_z(\omega))\,F_x(\omega)\cos^2\alpha \\ B &= F_z(2\omega)F_z^2(\omega)\sin^2\alpha \\ C &= F_z(2\omega)F_y^2(\omega) \\ D &= 4\left(\frac{\mu_0}{\epsilon_0}\right)^{3/2}\omega^2\tan^2\alpha \end{aligned}$$

where

P**:** angle denoting the polarization of the fundamental with respect to the plane of incidence

α**:** angle of incidence

μ_0**:** permeability constant

ϵ_0**:** permittivity constant

F_i: Fresnel factor as derived by the boundary conditions at the interfaces. The value is determined by the dielectric function of the individual layer and the angle of incidence α

The corresponding equation for an analyzer setting at $\hat{s}$ reads

$$I^{2\omega} = DF_y^2(2\omega)F_y^2(\omega)F_z^2(\omega)\sin^2(2P)|\chi^{(2)}_{yzy}|^2 I(2\omega)^2 \tag{2.10}$$

The unknown susceptibility components are the fit parameters. Alternatively, the orientation of the molecule can also be determined by two subsequent measurements of the intensity of SHG-light for $\hat{s}$ and $\hat{p}$-polarization of the incident beam.

$$\frac{\langle\cos^3\theta\rangle}{\langle\cos\theta\sin^2\theta\rangle} = \frac{\chi_{zzz}}{\chi_{zxx}} = -\frac{A}{2B} \pm \frac{C}{2B}\sqrt{\frac{I^{2\omega}(P=\hat{p})}{I^{2\omega}(P=\hat{s})}} \tag{2.11}$$

The correct sign (+/-) in eqn.(2.11) can be determined by an additional intensity measurement at a different polarizer setting.

2.3.9 SHG sample stage

Second harmonic generation experiments were carried out in reflection mode at a fixed angle of incidence of 53 degrees. The second harmonic beam of the pump laser was downtelescoped to 1.5 mm at the sample. All spurious SHG signals created by the optical components were removed by a visible cut-off filter (RG630, Schott) placed just in front of the sample. The frequency doubled light generated at the interface was separated from the fundamental by an IR-cutoff filter (BG39, Schott) in conjunction with a narrow band interference filter (532 BP, Instruments S.A.) and subsequently detected by a photomultiplier (C83068, Burle) with a quantum efficiency of 15%. The signal was amplified (V5D, Fa. Seefelder Messtechnik) and processed by a 500 MHz, 2 GSa/s digitizing oscilloscope (HP 54522 A, Hewlett Packard). All vital elements of the experiment are computer controlled. In order to eliminate experimental errors due to fluctuations in laser pulse intensity, the SHG-signal of a quartz crystal was used as a reference. The plane of polarization of the incident beam can be rotated by a Glan laser polarizer (extinction ratio 10^{-6}, PGL, Halle) and a low order quartz half wave plate

($\Delta\lambda = 0.001$, RLQ Halle). A polarization of 39° (the so called magic angle) with respect to the plane of incidence was used for the measurements of the number density. Under this condition orientational effects of the SHG active entity is minimized. The polarization of the reflected SHG-light can be analyzed by means of a Glan-Thomson prism (extinction ratio 10^{-6} ,Typ K, Fa. Steeg & Reuter).

2.4 Linear optics

2.4.1 Ellipsometry

Ellipsometry refers to a class of optical experiments which measure changes in the state of polarization upon reflection or transmission on the sample of interest. It is a powerful technique for the characterization of thin films and surfaces. In favorable cases thicknesses of thin films can be measured to within Å accuracy, furthermore it is possible to quantify submonolayer surface coverages with a resolution down to 1/100 of a monolayer. The high sensitivity is remarkable if one considers that the wavelength of the probing light is on the order of 500 nm. Many samples are suitable for ellipsometry and the only requirement is that they must reflect laser light. Its simplicity makes ellipsometry an ideal surface analytical tool for many objects in colloidal and interface science.

In the next two sections the basic equation of ellipsometry and how it can be applied to thin films is discussed. In section 2.4.4 it is shown that ellipsometric measurements allow a direct determination of the prevailing ion distribution. A simple analytical expression is derived, which can be used to retrieve the number of ions within the compact layer. The derived formalism relates the ellipsometric signal with the surface charge and a simple recipe is given to measure the condensation of counterions at a charged surface. Section 2.4.5 covers the experimental setup of a Nullellipsometer.

2.4.2 Basic equation of ellipsometry

A typical ellipsometric experiment is depicted in Figure 2.9. Light with a well defined state of polarization is incident on a sample. The reflected light

usually differs in its state of polarization and these changes are measured and quantified in an ellipsometric experiment.

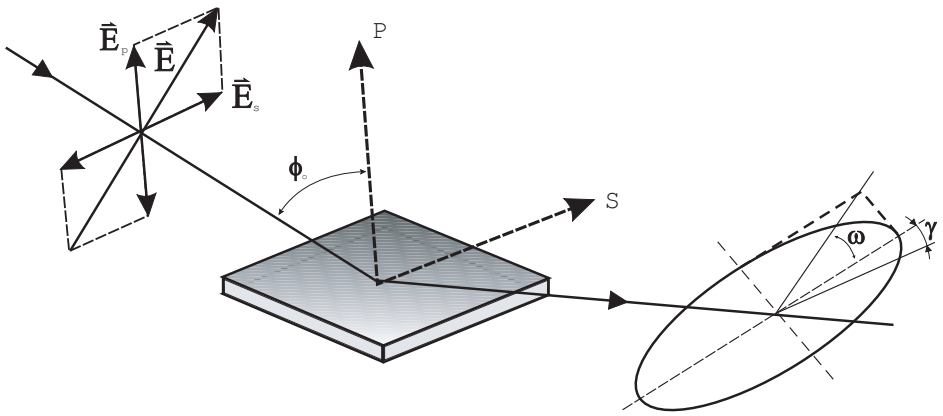

Figure 2.9: Ellipsometric experiment in reflection mode

The mathematical description is best done within the laboratory frame of reference defined by the plane of incidence. The propagation direction of the beam and the normal of the reflecting surface define the plane of incidence. Light with an electric field vector oscillating within the plane of incidence ($\hat{p}$-light) remains linearly polarized upon reflection and the same holds for $\hat{s}$-light with $\vec{E}$ perpendicular to the plane of incidence. For this reason $\hat{p}$- and $\hat{s}$-light are also called Eigen-polarizations of isotropic media or uniaxial perpendicular media. This consideration makes it obvious that this frame of reference is distinct. Incident and reflected beam can be described by the following vector:

$$\vec{E}_{\mathrm{inc}} = \begin{pmatrix} |E_{\mathrm{p}}^{\mathrm{i}}|e^{i\delta_{\mathrm{p}}^{\mathrm{i}}} \\ |E_{\mathrm{s}}^{\mathrm{i}}|e^{i\delta_{\mathrm{s}}^{\mathrm{i}}} \end{pmatrix} \qquad \vec{E}_{\mathrm{refl}} = \begin{pmatrix} |E_{\mathrm{p}}^{\mathrm{r}}|e^{i\delta_{\mathrm{p}}^{\mathrm{r}}} \\ |E_{\mathrm{s}}^{\mathrm{r}}|e^{i\delta_{\mathrm{s}}^{\mathrm{r}}} \end{pmatrix} \tag{2.12}$$

Two quantities Ψ and Δ are introduced in order to describe the changes in the state of polarization.

$$\Delta \;=\; (\delta_{\mathrm{p}}^{\mathrm{r}} - \delta_{\mathrm{s}}^{\mathrm{r}}) - (\delta_{\mathrm{p}}^{\mathrm{i}} - \delta_{\mathrm{s}}^{\mathrm{i}}) \tag{2.13}$$

$$\tan\Psi = \frac{|E_{\mathrm{p}}^{\mathrm{r}}|/|E_{\mathrm{p}}^{\mathrm{i}}|}{|E_{\mathrm{s}}^{\mathrm{r}}|/|E_{\mathrm{s}}^{\mathrm{i}}|} \tag{2.14}$$

Changes in the ratio of the amplitudes are described as the tangent of the angle Ψ.

The reflectivity properties of a sample within a given experiment are given by the corresponding reflection coefficients r_p and r_s. The reflection coefficient is a complex quantity that accounts for changes in phase and amplitude of the reflected electric field E^{r} with respect to the incident one E^{i}.

$$r_{\mathrm{p}} = \frac{|E_{\mathrm{p}}^{\mathrm{r}}|}{|E_{\mathrm{p}}^{i}|} e^{i(\delta_{\mathrm{p}}^{\mathrm{r}} - \delta_{\mathrm{p}}^{i})} \qquad r_{\mathrm{s}} = \frac{|E_{\mathrm{s}}^{\mathrm{r}}|}{|E_{\mathrm{s}}^{i}|} e^{i(\delta_{\mathrm{s}}^{\mathrm{r}} - \delta_{\mathrm{s}}^{i})} \tag{2.15}$$

Interference cannot be observed between orthogonal beams and hence $\hat{p}$- and $\hat{s}$-light do not influence each other and can be separately treated. With these definitions the basic equation of ellipsometry is obtained

$$\tan\Psi \cdot e^{i\Delta} = \frac{r_{\mathrm{p}}}{r_{\mathrm{s}}} = \rho = \Re(\rho) + i\Im(\rho) \tag{2.16}$$

Eq 2.16 relates the quantities Ψ and Δ with the reflectivity properties of the sample.

2.4.3 Ellipsometry applied to the air/water interface

In the case of adsorption layers of nonionic surfactants at the air/water interface, there is a striking mismatch between interfacial height h and the wavelength of light λ. As a result certain peculiarities exist which are discussed in this section [15].

The most striking limitation is a reduction of the measurable quantities. The presence of an organic monolayer (refractive index 1.3-1.6) with a thickness below 2.5 nm does not change the reflectivity $|r_i|^2$ and as a consequence there are no detectable changes in Ψ. In the thin film limit $h \ll \lambda$ the data analysis relies only on a single parameter, namely changes in the phase Δ. Unfortunately the number of independent data cannot be increased. Neither spectroscopic ellipsometry nor a variation of the angle of incidence yield

new independent data, instead all quantities remain strongly coupled. A profound treatment is given in [16]. However, the sensitivity of an ellipsometric measurement can be significantly increased by the choice of the angle of incidence.

The exact formula relating the reflectivity coefficients of a single homogeneous layer with refractive index $n_1 = \sqrt{\epsilon_1}$ in between two infinite media ($n_0 = \sqrt{\epsilon_0}$ and $n_2 = \sqrt{\epsilon_2}$) at an angle of incidence φ is given by :

$$\Delta = \arctan \frac{Im\left(\frac{r_p}{r_s}\right)}{Re\left(\frac{r_p}{r_s}\right)} \qquad \text{with} \qquad \begin{aligned} r_p &= |r_p| \cdot e^{i\delta_{r,p}} = \tfrac{r_{0,1,p}+r_{1,2,p}e^{-i2\beta}}{1+r_{0,1,p}r_{1,2,p}e^{-i2\beta}} \\ r_s &= |r_s| \cdot e^{i\delta_{r,s}} = \tfrac{r_{0,1,s}+r_{1,2,s}e^{-i2\beta}}{1+r_{0,1,s}r_{1,2,s}e^{-i2\beta}} \end{aligned} \tag{2.17}$$

where the reflectivity coefficients $r_{0,1,p}$, $r_{1,2,p}$, $r_{0,1,s}$ and $r_{1,2,s}$ describing the reflection at refractive index jumps $n_0 \rightarrow n_1$ and $n_1 \rightarrow n_2$ for $\hat{p}$- and $\hat{s}$-light are given by Fresnel's laws. $\beta = 2\pi\frac{h}{\lambda}\sqrt{n_1^2 - n_0^2 \sin^2\varphi}$ accounts for the phase shift occurring in a single pass within the adsorption layer.

If the layer thickness h is much smaller than the wavelength λ of light it is justified to expand the complex reflectivity coefficients in a power series in terms of h/λ. The first term in this expansion describes reflection at a monolayer.

$$\Delta \approx \frac{4\sqrt{\epsilon_0}\epsilon_2\pi\cos\varphi\sin^2\varphi}{(\epsilon_0-\epsilon_2)((\epsilon_0+\epsilon_2)\cos^2\varphi-\epsilon_0)} \cdot \frac{(\epsilon_1-\epsilon_0)(\epsilon_2-\epsilon_1)}{\epsilon_1} \cdot \frac{h}{\lambda} \tag{2.18}$$

If the refractive index is varying over the height of the layer, the term

$$\frac{(\epsilon_1-\epsilon_0)(\epsilon_2-\epsilon_1)}{\epsilon_1} \cdot h$$

within eq 2.18 has to be replaced by an integral η across the interface:

$$\eta = \int \frac{(\epsilon-\epsilon_0)(\epsilon_2-\epsilon)}{\epsilon}\, dz \tag{2.19}$$

An ellipsometric experiment on a monolayer yields a quantity proportional to η. This equation is used for a further analytical simplification in order to quantify the impact of the counterions in the diffuse layer as outlined in the next section.

2.4.4 Impact of the diffuse layer on the ellipsometric angle Δ

The condensed counterions in the compact layer reduce the surface charge density and influence the counterion distribution in the diffuse layer. The distribution of the counterions is only a function of the effective surface charge density σ as soon as the parameter γ (section 1.1.3) exceeds a value of 0.8. The relation is then described by eq 1.2. Because of the linear relation between the dielectric function and the concentration in the diffuse layer we can translate the ion distribution into a refractive index profile:

$$\epsilon(z) = \epsilon_2 + c(z)\frac{\mathrm{d}\epsilon}{\mathrm{d}c} = \epsilon_2 + \frac{1}{2\pi l_B N_A (z+b)^2}\frac{\mathrm{d}\epsilon}{\mathrm{d}c} \tag{2.20}$$

where N_A is Avogadros constant. To quantify the impact of the counterion distribution in the diffuse layer on the ellipsometric angle Δ we separate the integral over the interface in eqn.(2.19):

$$\begin{aligned} \eta &= \int_0^d \frac{(\epsilon-\epsilon_0)(\epsilon-\epsilon_2)}{\epsilon}\,dz + \int_d^a \frac{(\epsilon-\epsilon_0)(\epsilon-\epsilon_2)}{\epsilon}\,dz \\ &= \eta_{SL} + \eta_{DL} \end{aligned} \tag{2.21}$$

where the second term η_{DL} describes the influence of the counterions in the diffuse layer. The length d is the thickness of the stern layer. Ellipsometry probes the system off-resonant at optical frequencies (10^{15}Hz). If the adsorption process does not form new species with new electronic signatures the polarizability at optical frequencies remains unchanged. Hence η_{SL} is dominated by the adsorbed surfactants and not significantly changed upon ion condensation. Note that the dielectric constant of the layer consisting of the surfactants is typically about 2.2. Inserting eq 2.20 in the integral η_{DL} and transforming the variable $\varepsilon(z) \rightarrow \epsilon(z-d)$ leads to

$$\eta_{DL} = \int_0^{a-d} \frac{(\epsilon_2 - \epsilon_0 + \frac{\frac{\mathrm{d}\epsilon}{\mathrm{d}c}}{2\pi l_B N_A (z+b)^2})(\frac{\frac{\mathrm{d}\epsilon}{\mathrm{d}c}}{2\pi l_B N_A (z+b)^2})}{\epsilon_2 + \frac{\frac{\mathrm{d}\epsilon}{\mathrm{d}c}}{2\pi l_B N_A (z+b)^2}}\,dz \tag{2.22}$$

with further simplifications:

$$\eta_{DL} = \int_0^{a-d} \frac{\frac{\mathrm{d}\epsilon}{\mathrm{d}c}(\epsilon_2 - \epsilon_0 + \frac{\frac{\mathrm{d}\epsilon}{\mathrm{d}c}}{2\pi l_B N_A (z+b)^2})}{2\pi l_B N_A (z+b)^2(\epsilon_2 + \frac{\frac{\mathrm{d}\epsilon}{\mathrm{d}c}}{2\pi l_B N_A (z+b)^2})}\, dz \tag{2.23}$$

$$= \int_0^{a-d} \frac{\frac{\mathrm{d}\epsilon}{\mathrm{d}c}(\frac{\mathrm{d}\epsilon}{\mathrm{d}c} - (\epsilon_0 - \epsilon_2)2\pi l_B N_A (z+b)^2}{2\pi l_B N_A (z+b)^2(\frac{\mathrm{d}\epsilon}{\mathrm{d}c} + \epsilon_2 2\pi l_B N_A (z+b)^2)}\, dz. \tag{2.24}$$

The ellipsometric signal is sensitive to changes in the dielectric function. Therefore the upper bound $(a-d)$ must resemble the distance r in the solution, where the dielectric function reaches the value of ϵ_2. Since the integration of η_{DL} to higher distances r does not change the value of η_{DL}, we just have to choose a sufficient length r. With these deliberations we found the following solution of eq 2.24:

$$\eta_{DL} = \frac{\frac{d\epsilon}{dc}(b-r)}{2\pi l_B N_A b \cdot r} + k\epsilon_0 \cdot \left(\arctan\left(\frac{r}{k}\right) - \arctan\left(\frac{b}{k}\right)\right) \tag{2.25}$$

with

$$k = \sqrt{\frac{\frac{d\epsilon}{dc}}{2\pi l_B N_A \epsilon_2}} \tag{2.26}$$

The limiting value of the ellispometric moment η reads:

$$\eta_{DL} = \lim_{r\to\infty} \eta_{DL} = -\frac{\frac{d\epsilon}{dc}}{2\pi l_B N_A \cdot b} + k\epsilon_0 \cdot \left(\frac{\pi}{2} - \arctan\left(\frac{b}{k}\right)\right) \tag{2.27}$$

With the relation $b = e/(2\pi\sigma l)$ we derive the following expression describing the influence of the diffuse layer on the ellipsometric angle Δ:

$$\eta_{DL} = -\frac{d\epsilon}{dc} \cdot \frac{\sigma}{eN_A} + k\epsilon_0 \cdot \left(\frac{\pi}{2} - \arctan\left(\frac{e}{\sigma}\sqrt{\frac{\epsilon_2 N_A}{2\pi l_B \frac{d\epsilon}{dc}}}\right)\right) \tag{2.28}$$

This equation in combination with the prefactor of eq 2.18 describes the ellipsometric response of the distribution of the counterions within the diffuse layer. It can be used to retrieve the effective surface charge density σ

and contains only directly measurable quantities. Experimentalists can use this formula for a straightforward interpretation of measured ellipsometric isotherms for ionic surfactants at the air-water interface. The relation is plotted in Figure 2.10 for bromide, chloride and fluoride.

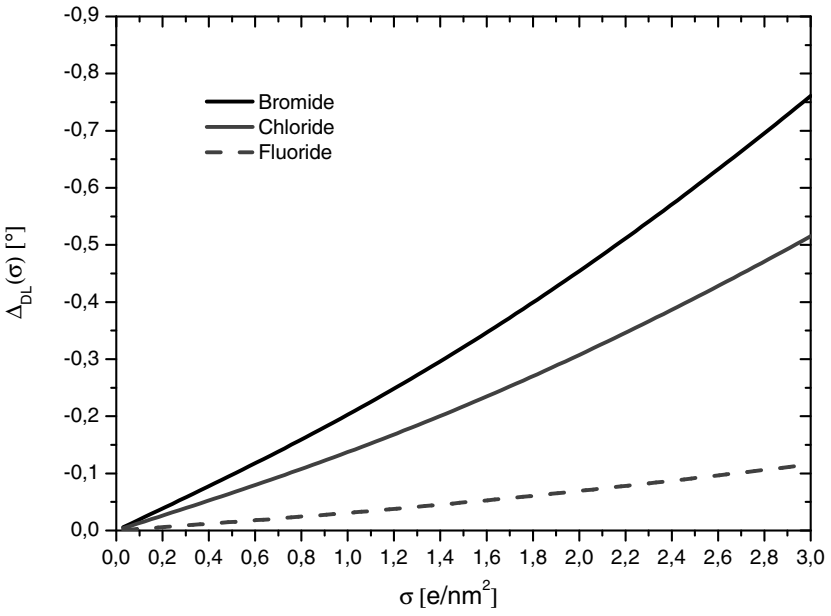

Figure 2.10: The impact of the counterions in the diffuse layer on the ellipsometric angle Δ in dependence of the prevailing surface charge density of the compact layer for different counterions. The dielectric constant increment of potassium bromide ($\mathrm{d}\epsilon/\mathrm{d}c = 3.453 \cdot 10^{-5}\mathrm{m}^3/\mathrm{mol}$), potassium chloride ($\mathrm{d}\epsilon/\mathrm{d}c = 2.411 \cdot 10^{-5}\mathrm{m}^3/\mathrm{mol}$) and potassium fluoride ($\mathrm{d}\epsilon/\mathrm{d}c = 3.586 \cdot 10^{-6}\mathrm{m}^3/\mathrm{mol}$) was used for the calculations. The angle of incidence was $\varphi = 56°$ and the dielectric constant of air $\epsilon_0 = 1.0$ and water $\epsilon_2 = 1.77$ was used. [18, 19]

The impact of the compact layer η_{SL} on the ellipsometric angle Δ is dominated by the amphiphiles and scales linearly with the surface coverage. Therefore any deviation from linearity can be attributed to changes in the distribution of the counterions.

The procedure for the determination of the ion distribution on the basis of eq 2.28 can be reduced to a simple recipe: 1) Determine the surface coverage Γ by an independent technique. It is for instance given by the derivative of the surface tension isotherm. There is a linear relation between the surface coverage and ellipsometric angle Δ provided that all counterions are located in the diffuse layer. 2) Measure carefully the ellipsometric isotherm with a high precision ellipsometer. Deviations from the linearity of a Δ versus Γ plot can be attributed to changes in the counterion distribution. A comparison of the deviations with Figure 2.10 yields directly the effective charge density of the surface layer which can alternatively be expressed as the number of condensed counterions.

At monolayer coverage the ellipsometric signal is usually on the order of 2° and therefore the impact of the counterions in the sublayer on the ellipsometric angle can be up to 25%. However, to ensure sublayer sensitivity in the ellipsometric signal all experiments were carefully done on a shockfree table with a high purified stock solution as indicated in section 2.2. The measurements of surface tension, ellipsometry and SHG were done with the same stock solution one after the other on the same day.

2.4.5 Experimental design

Many different designs of ellipsometers have been suggested and a good overview is presented in Azzam and Bashara [17]. Here we discuss common roots of all arrangements and the underlying theory.

The layout of a typical ellipsometer is depicted in Fig. 2.11. The main components are a polarizer P which produces linearly polarized light, a compensator C which introduces a defined phase retardation of one field component with respect to the orthogonal one, the sample S, the analyzer A and a detector.

This setup allows the determination of the unknown ellipsometric angles and can be operated in various modes. The unknown reflectivity coefficients

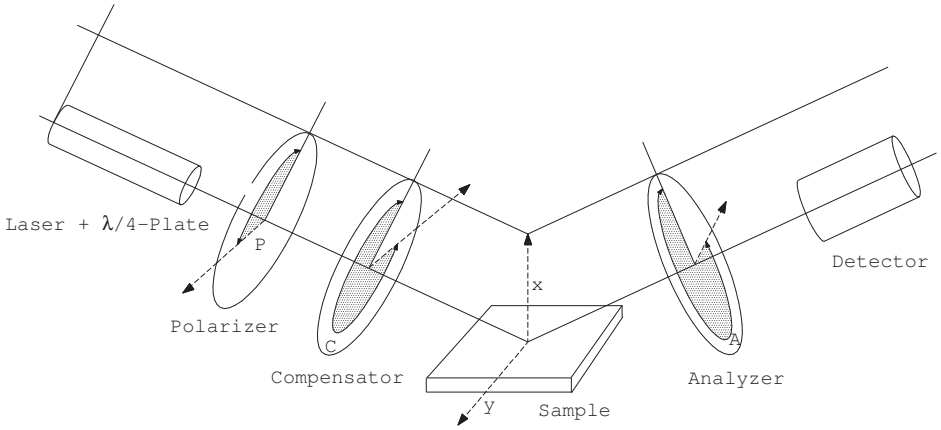

Figure 2.11: Ellipsometer in a PCSA-configuration

can be retrieved in various manners and the applied measurement scheme names the method. *Rotating analyzer* means recording the intensity as a function of the setting of the analyzer and work out the unknown ellipsometric angles by a Fourier analysis. *Polarization modulation* ellipsometry uses a variable phase retardation δ_c for a calculation of the ellipsometric angles. Polarization modulation uses an electro-optic or acusto-optic modulator driven at a high frequency. The measurement is fast, however, there are also some inherent problems due to an undesired interferometric contribution of the modulator to the signal which cannot be separated from the contribution of the sample. The technique is very well suited to follow relative changes.

A particularly successful implementation is *Nullellipsometry* which eliminates many intrinsic errors due to slight misalignments of the sample. Within Nullellipsometry the setting of the optical components is chosen such that the light at the detector vanishes. A given elliptical state of polarization of the incident light leads to linear polarized light after reflection and can be completely extinguished with an analyzer. The following equation relates the reflectivity coefficients r_p and r_s to the settings of the components [20]:

$$\frac{r_\mathrm{p}}{r_\mathrm{s}} = -\tan A \frac{\tan C + \rho_c \tan(C-P)}{1 - \rho_c \tan C \tan(C-P)} \tag{2.29}$$

for a vanishing intensity $I = 0$ at the detector. This equation can be further simplified by using a high precision quarter waveplate as a compensator

($t_C = 1$, $\delta_C = \pi/2 \Longrightarrow \rho_c = -i$) fixed to $C = \pm 45°$. With eqn. (2.16) a further simplification of the eqn. (2.29) can be achieved.

$$\begin{aligned} \tan\Psi e^{i\Delta} = \frac{r_\mathrm{p}}{r_\mathrm{s}} &= \tan A_0 \exp[i(2P_0 + \frac{\pi}{2})] \qquad \text{if} \quad C = -45° \\ \tan\Psi e^{i\Delta} = \frac{r_\mathrm{p}}{r_\mathrm{s}} &= -\tan A_0 \exp[i(\frac{\pi}{2} - 2P_0)] \qquad \text{if} \quad C = 45° \end{aligned} \tag{2.30}$$

Eqn. (2.30) links the quantities Δ and Ψ to the null settings of the polarizer P_0 and analyzer A_0. Once a setting ($P_0,\ A_0$) has been determined which provides a complete cancellation of the light, then the same holds for the pair ($\tilde{P}_0,\ \tilde{A}_0$).

$$(\tilde{P}_0,\ \tilde{A}_0) = (P_0 + 90°,\ 180° - A_0) \qquad \text{if} \quad I = 0 \quad \text{for} \quad (P_0,\ A_0) \tag{2.31}$$

These nontrivial pairs of nullsettings are refered as ellipsometric zones. Measurements in various zones lead to a high accuracy in the determination of absolute values. Many intrinsic small errors due to misalignment are cancelled by this scheme.

All relevant design features of the ellipsometer (Multiskop, www.optrel.de) are discussed in Ref. [21]. We used the Null ellipsometer mode of the ellipsometry module in a laser, polarizer, compensator, sample, analyzer arrangement at an angle of incidence of 56°.

2.5 The oscillating bubble device

The principle of the oscillating bubble technique is sketched in Figure 2.12 showing a cross sectional view of the chamber.

A small hemispherical bubble is formed at the tip of a capillary with a radius of about 0.2 mm. The bubble is forced in a sinusoidal oscillation by a piezoelectric translator which is directly immersed in the liquid. As a result, a harmonic modulation of the pressure in the chamber is observed and recorded by a sensitive pressure transducer located at the bottom of the chamber.

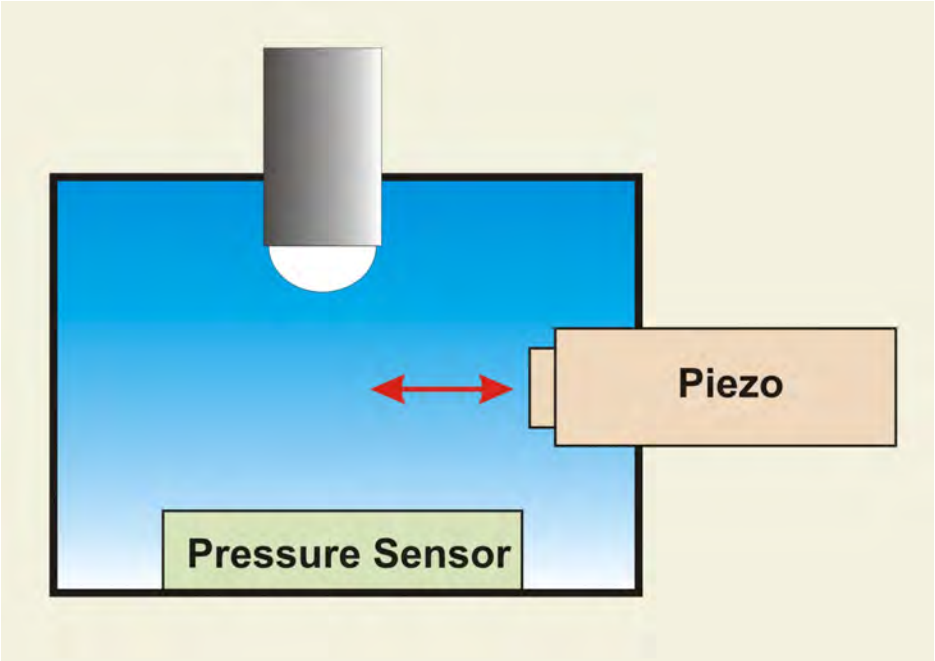

Figure 2.12: Cross sectional view of the oscillating bubble device. The piezo translator is immersed in the liquid, the bubble is formed at the tip of the capillary and the pressure is recorded by a sensitive pressure transducer at the bottom of the chamber. The piezo movement leads to an expansion and compression of the surface layer.

The amplitude of the pressure response and the phase-shift between piezo oscillation and pressure signal are evaluated via a phase sensitive lock-in detection scheme. The amplitude of the pressure response is proportional to the magnitude of the complex surface dilational modulus E, while the phase-shift yields the imaginary part of the modulus, in other words the surface dilational viscosity.

The experimental arrangement allows a precise determination of real and imaginary part of the complex E module. In particular the experiment yields the high frequency limit of the E module, a quantity previous measurements are lacking [22]. Only the analysis of two well defined harmonic signals is required: the piezo oscillation and the pressure signal. A Fourier analysis of the pressure response reveals that there are no higher harmonic waves in the signal. Hence, the phase between the harmonic piezo oscillation and

the harmonic pressure response can be measured with high accuracy. It was claimed that it is not possible to maintain a zero order mode for a rapidly oscillating bubble [23, 24]. For this reason, we investigated the system with a high speed camera at 2000 frames per second. The video analysis proves that the bubble indeed oscillates in the zero order mode up to 1000 Hz. Secondly we could verify the stability of the three phase contact line and hence the relative area changes $\Delta A/A$ remain well defined at all frequencies. A crucial step to achieve the desired performance is the treatment of the capillary: the capillary is silanized and then cleaved leading to a sharp hydrophilic/hydrophobic boundary that keeps the bubble in place during the duration of the experiment.

The piezo driver fulfils two functions, the static DC-voltage V_{DC} controls the bubble shape and ensures the maintenance of the half sphere geometry during the course of the experiment, the overlaid oscillating AC-voltage forces the bubble in a sinusoidal oscillation.

$$V_{\mathrm{Piezo}} = V_{\mathrm{DC}} + V_{\mathrm{AC}} \sin(2\pi\nu t) \tag{2.32}$$

The relative area change $\Delta A/A$ is about ± 5 percent. The experimental arrangement suppresses several unwanted effects such as a Marangoni flow and allows a sound modeling of the underlying processes. The stable three contact line of the capillary and the direct measurement of the pressure within the chamber gives access to a frequency range of 1 Hz to 500 Hz with room for further extensions in both directions.

The change of the bubble size modifies the pressure within the chamber. The measured pressure response is harmonic, however, the signal can be phase shifted by an angle ϕ with respect to the piezo oscillation.

$$p(t) = p^0 + \tilde{p} \sin(2\pi\nu t + \phi) \tag{2.33}$$

The pressure difference $\Delta p = p(t) - p^0$ in the chamber has the following contributions [25]:

$$\Delta p = -\frac{2}{r_0}\Delta\gamma + 2\frac{\gamma}{r_0^2}\Delta r + H(f) \tag{2.34}$$

Δr describes the deviation of the bubble radius r from the half-sphere r_o,

$\Delta\gamma$ denotes the change in the interfacial tension γ and $H(f)$ captures the influence of hydrodynamics, bulk viscosity and inertia.

The frequency dependent hydrodynamic term $H(f)$ contributes only at frequencies exceeding 200 Hz. In principle it is possible to estimate $H(f)$ by first principles as outlined in [26]. A sound alternative are calibration measurements using a well characterized component such as decanoic acid which behaves completely elastic. In this case, the limiting value of the E-modulus is reached at moderate frequencies ($\approx$ 100 Hz) and the experimentally observed decrease of the pressure amplitude at higher frequencies can be attributed to the hydrodynamic correction term $H(f)$ which can be used for the normalization of subsequent measurements.

The system is completely controlled by a computer. The piezo motion is controlled by an AD-DA converter which processes also the amplified signal of the pressure sensor. Bubble and capillary are imaged by a microscope, digitized and processed in a personal computer. The video system is crucial for maintaining the bubble size which is required for the compensation of thermal drifts within the chamber.

An excellent assessment for the quality and purity of the chamber is the measurement of pure water. Since water possesses neither a surface elasticity nor a surface viscosity, the pressure response is dominated by the second term of eq 2.34. Consequently the oscillation at half sphere geometry leads then to a frequency doubling of the pressure response. This probes the state of the chamber because frequency doubling is not observed in the presence of any surface active trace impurities.

2.6 Foam stability measurement

The foam lamella stability was measured using the method proposed by Gilanyi et al. [27]. Foam lamellae were produced in a rectangular glass frame with a size of 50 x 40 mm. The lamella is in direct contact with the aqueous surfactant solution in a closed housing under saturated humidity. Figure 2.13 shows a photograph of the device. The lifetime of the surface is visually observed. Measurements are at least 20 times repeated to ensure a reliable statistics.

Figure 2.13: Photo of the device used for the measurement of the lamella lifetime.

2.7 Surface Tension

The spontaneous adsorption of surface active agents (surfactants) in a monolayer at the interface leads to a decrease in the equilibrium surface tension compared to the bare air/water interface. At bulk concentrations usually in the mmol/L regime the surface tension becomes almost constant and thus the interface remains virtually unchanged. Starting from this so called critical micelle concentration (cmc) the amphiphiles selfaggregate to microphases in which the hydrophobic chains sequester themselves inside the aggregate (micelles, vesicles or planar bilayers) and the polar headgroups orient themselves toward the aqueous phase. Since we are interested in the static and dynamic properties of Gibbs monolayers all experiments where done at concentrations below the cmc (c= 4 mmol/L for C12-DMPB).

With a ring tensiometer (model K11, Krüss) the equilibrium surface tension γ_e was recorded. The critical micelle concentration was determined on the basis of the adsorption isotherm. The *cmc* values of the members of the homologous series strictly follow the Stauff-Klevens equation [28].

Bibliography

[1] K. Haage, H. Motschmann, S. Bae, Egon Gründemann *Colloids and Surfaces* **183**, 583, (2001)

[2] Elworthy, P.H.; Mysels, K.J. *J. Colloid Interface Sci.* , 331, (1966).

[3] Mysel, K.; Florence, A.; *J. Coll. Int. Sci.* , **43**, 577, (1973).

[4] Lunkenheimer, K. *J. Colloid Interface Sci.* **1989**, *131*, 580

[5] Lunkenheimer, K; Pergande, H.J.; Krüger, H. *Rev. Sci. Instrum.* **1987**, *58* , 2313.

[6] Shen, Y.R. *Ann. Rev. Phys. Chem* **1989**, *40*, 327.

[7] G. L. Richmond *Chem. Rev.* **2002**,*102*, 2693.

[8] Corn, R.,M.; Higgins, D.A. *Chem. Rev.* **1994**, *94*, 107.

[9] Bae, S.; Haage, K.; Wandtke, D.; Motschmann, H. *J. Phys. Chem. B.* **1999** *103(7)*, 1045.

[10] Vogel, V; Mullin, C; Shen, Y.R., Kim, M.W. *J. Chem. Phys.* **1995**, *95*, 4620.

[11] Prasad, P.; Williams, D.J. *Introduction to Nonlinear Optical Effects in Molecules and Polymers*; Wiley: New York, **1991**.

[12] Goldstein, H: *Classical Mechanic* Addison Wesley, London (1981)

[13] Hirose, C; Akamatsu, N; Domen, K. *Applied Spectroscopy* (1992), **6** , 1051.

[14] Harke, M.; Ibn Elhaj, M.; Möhwald, H.; Motschmann, H. *Phys. Rev. E*, **1998**, *57*, 1806,

[15] R. Teppner, S. Bae, K. Haage, H. Motschmann *Langmuir* , **15**, 7002, (1999).

[16] R. Reiter, H. Motschmann, H. Orendi, A. Nemetz, W. Knoll *Langmuir* **8**, 1784, (1992).

[17] R. M. Azzam, N.M. Bashara *Ellipsometry and Polarized Light* North Holland Publication, Amsterdam, (1979).

[18] Koelsch, P.; Motschmann, H. *Current Opinion in Colloid and Interface Science*, 9 (2004) 87-91.

[19] Koelsch, P.; Motschmann, H. *J. Phys. Chem. B* 2004, 108(48),18659-18664.

[20] R.C. Jones *J. Opt. Soc. Am* **16**, 488, (1941).

[21] M. Harke, R. Teppner, O. Schulz, H. Orendi, H. Motschmann *Rev. Sci. Instrum.*,**68**, 8, 3130, (1997).

[22] C. Stubenrauch, R. Miller, J. Phys. Chem. B 2004, 108, 6412-6421

[23] V. I. Kovalchuk, J. Krägel, A. V. Makievski, G. Loglio, F. Ravera, L. Liggieri, and R. Miller, 1 Journal of Colloid and Interface Science 252, 433 (2002)

[24] V I. Kovalchuk, E. K. Zholkovskij, J. Krägel, R. Miller, V. B. Fainerman, R.Wüstneck, G. Loglio, S. S. Dukhin Journal of Colloid and Interface Science 224, 245254 (2000)

[25] K.-D. Wantke, H. Fruhner, J. Oertegren Colloids and Surfaces A: Physicochem. Eng. Aspects 221 (2003) 185

[26] K. Wantke, H. Fruhner Journal of Colloid and Interface Science 237, 185-199 (2001)

[27] T. Gilanyi, C. Stergiopulos, E. Wolfram, Colloid Polym. Sci. 254 (1976) 1018.

[28] Stauff, J; *Kolloidchemie*, Springer, Berlin, **1960**.

Chapter 3

Results and Discussion

3.1 Ion distribution at charged interfaces

3.1.1 Varying the counterions at a charged interface

The influence of different counterions on the adsorption behavior of the ionic soluble surfactant dodecyldimethylammonium- pyridimium bromide is investigated. The addition of potassium halogenides to aqueous solutions of the surfactant modifies the surface activity of the amphiphile and has a profound influence on the surface tension isotherms. In order to gain direct structural information surface second harmonic generation and ellipsometry have been applied. The combination of both optical techniques yields the number density of the condensed counterions within the compact layer.

Infrared-Visible sum frequency spectroscopy was used to study the structure of the interfacial water and the vibrational alkyl stretching modes of both distinct surface phases. Furthermore the influence of an indifferent electrolyte on both surface states is investigated.

3.1.2 Surface tension measurements

The experimental equilibrium surface tension isotherms (surface tension γ_e versus bulk concentration) of the cationic amphiphile C12-DMPB is represented by the stars in Figure 3.1. The amphiphile is a strong electrolyte and

the conductivity follows the prediction of the Debye-Hückel theory [2]. The surface tension isotherm shows a critical micelle concentration at a surface tension of 43 mN/m.

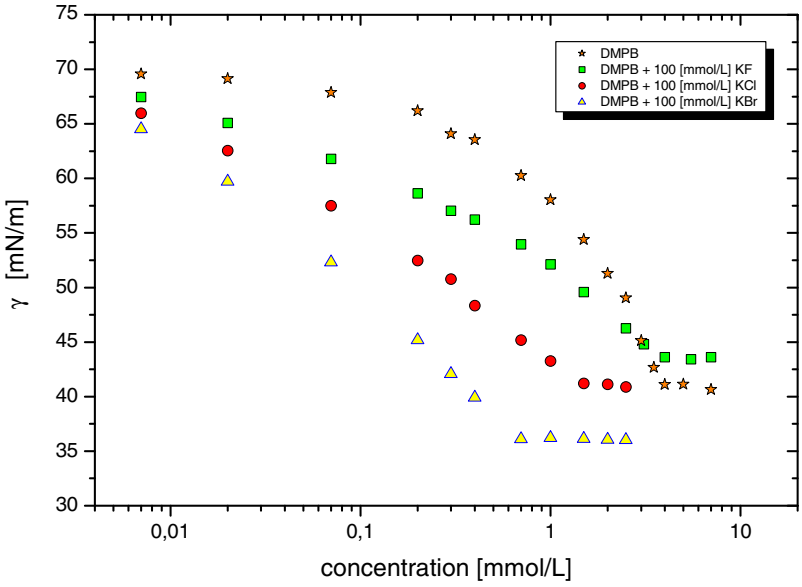

Figure 3.1: Surface tension isotherms of C12-DMPB for the pure solution (stars) and the solutions where 100 mmol/L of KBr (triangles), KCl (circles) and KF (square) was added to each concentration of the surfactant. The cmc observed for different counterions follows the order of the periodic table of elements. [1]

The measured critical micelle concentration derived from the break in the isotherm slopes follows the order of the periodic table of elements.

In order to investigate the influence of indifferent electrolytes on the system behavior, KBr, KCl, and KF was added to a portion of the purified stock solution and the equilibrium surface tension isotherms were again measured. The total concentration of the indifferent electrolyte was 100 mM, exceeding the concentration of the amphiphile by a factor of 100-1000. The indifferent electrolyte has a strong impact on the corresponding isotherms as shown in Figure 3.1: bromide (triangles), chloride (circles), and fluoride (squares).

The salt increases the surface activity; the cmc derived from the break in the isotherm slopes is shifted to lower concentrations and occurs at different surface tensions: 35 mN/m for KBr, 42 mN/m for KCL, and 45 mN/m for KF. Obviously there is an ion specificity in the system behavior. The decrease in the surface tension comparing the different added counterions follows the order of the periodic table of elements. Fluoride has the smallest impact on the surface tension followed by chloride and bromide. Because most molecular properties such as ion radius, polarizability and hydration energy possess a monotonic behavior within a period one can speculate about a fundamental correlation.

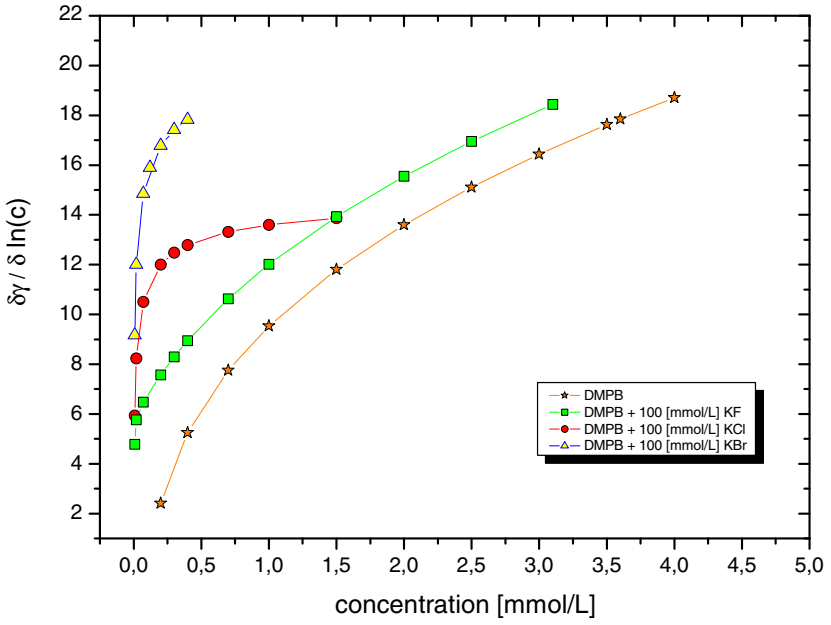

Figure 3.2: Derivative of of the surface tension isotherms. The values for the pure solution were normalized by the factor m. The order at the cmc does not follow the periodic table. [1]

The surface excess can be retrieved by analyzing the isotherm in the framework of Gibb's equation. The slope of the surface tension isotherm is proportional to the total surface excess [3]:

$$\Gamma = -\left(\frac{\partial \gamma_e}{\partial \mu}\right)_T = -1/(mRT)\frac{\mathrm{d}\gamma_e}{\mathrm{d}\ln a} \approx -1/(mRT)\frac{\mathrm{d}\gamma_e}{\mathrm{d}\ln c} \qquad (3.1)$$

where μ is the chemical potential of the solute component in the bulk solution, m is the number of independent components, and a is the activity of the solute. Because the concentration of soluble surfactants in the range below the cmc is very low it is justified to replace the activity by the bulk concentration c [3]. In absence of an indifferent electrolyte the rigorous thermodynamical treatment requires a factor of $m = 2$ for a 1:1 ionic surfactant provided that the system is completely dissociated in the surface phase following an ideal behavior. The derivative of the interfacial tension as a function of the bulk concentration is presented in Figure 3.2 on a linear scale. The most surprising finding is that the surface excess does not follow at all the order of the periodic table of elements as the surface tension does. It is remarkable that the functional dependence of the slope of the surface excess for fluoride matches the values of the pure solution. This implies that obviously fluoride has negligible impact on the adsorption of the surfactant despite the fact that the slope of the surface tension isotherm is changed. Furthermore, it is noticeable that the surface excess at the cmc seems to be independent of the amount of counterions because the surface excess for the solution with added counterions of bromide matches the one of the pure solution.

3.1.3 Second harmonic generation measurements

To gain a more detailed picture of the interfacial architecture we performed linear and nonlinear optical measurements. As outlined in section 2.3.8, surface SHG is a nonlinear optical technique with an inherent surface specificity. Only the adsorbed surfactant molecules that contribute to the signal and bulk contributions are suppressed. The SHG response is completely dominated by the surfactant headgroup because this moiety dominates the hyperpolarizability due to the π push-pull system. Polarization dependent SHG measurements [4] reveal that (a) the orientational order of the headgroup is independent of the surface coverage with a tilt angle of 59° of the long chromophore axis with respect to the surface normal and (b) the symmetry of the molecular arrangement of the headgroup belongs to the point

group $C_{\infty v}$ which is characteristic for an isotropic azimuthal arrangement within the adsorption layer.

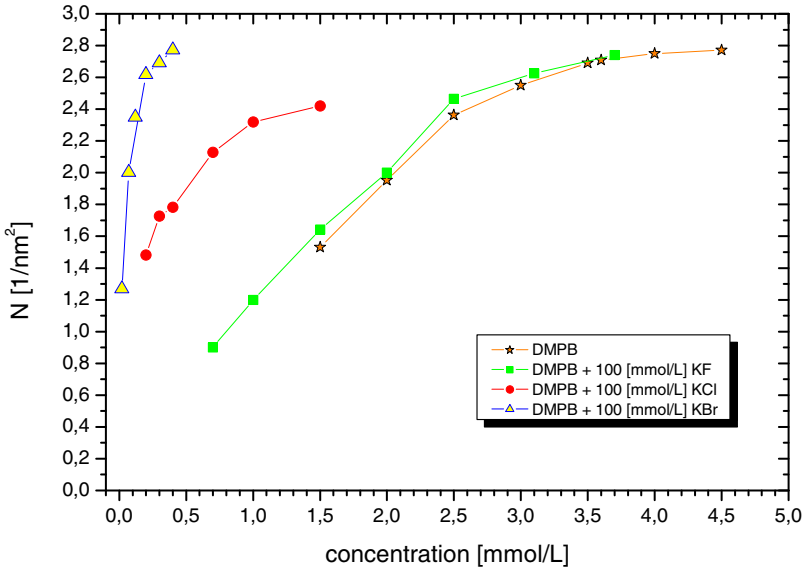

Figure 3.3: Number density N of the surfactants measured by surface second harmonic generation. Fluoride has no impact on the adsorption behaviour of the surfactant. The number density at the cmc for the pure solution is equal to the one where KBr was added. [1]

The absolute number density of the cationic amphiphile requires the evaluation of SHG intensities. There is a direct relation between SHG intensity and number densities of the headgroup; however, the underlying expression is complex because of the difficulty to account for local field corrections. A rock solid alternative has been developed in [4]. The SHG signal is properly calibrated using a Langmuir monolayer of the water-insoluble C20 representative of the homologous series. The number density of a quasi-two-dimensional Langmuir layer is directly given by the preparation, and also all effects and inherent ambiguities are then eliminated. The orientational order of the water-insoluble C20 amphiphile was identically verified to the C12 representative at the desired surface coverages.

The results of the calibrated SHG measurements are presented in Figure 3.3. It shows the number density of the surfactant headgroup as a function of the bulk concentration. SHG records the adsorbed headgroups without a discrimination between adsorbed ion pairs and adsorbed amphiphile. The formation of the ion pairs does not form new species with a new electronic signature at optical frequencies; hence, the hyperpolarizibility is not changed by the formation of ion pairs.

The SHG measurement goes nicely along with the analysis of the surface tension isotherm. The SHG intensity measurements reveal that the surfactant surface coverage of the pure surfactant is not altered by adding fluoride as the counterion. Furthermore, the limiting value for the surfactant surface coverage is independent of the amount of counterions in the solution, because the values for the pure solution and the solution with the added bromide are nearly identical at the cmc. This is in accordance with the analysis of the surface tension isotherms, only chloride as a counterion decreases the surface coverage.

3.1.4 Ellipsometric measurements

Further details on the ion distribution can be retrieved by ellipsometry which records the complete transition region between air and the aqueous surfactant solution. The ellipsometric isotherm of the system is displayed in Figure 3.4.

The optical isotherms are showing a monotonic increase with the bulk concentration. The difference to the SHG isotherms is obvious because in the limiting values it depends on the nature of the counterion. Specifically, the ellipsometric angle Δ of the pure solution and the solution with fluoride as a counterion at the cmc is significantly lower as compared to that of bromide. It is already established that in the case of nonionic surfactants the ellipsometric angle Δ is proportional to the surface coverage [5]. This must not be the case for ionic surfactants because ellipsometry is also sensitive to the distribution of the counterions.

The ellipsometric isotherm can be used to retrieve the number density of the condensed counterions. The procedure for the determination of the ion distribution on the basis of eq 2.28 can be reduced to a simple recipe: First, determine the surface coverage $\Gamma(c)$ as a function of the surfactant

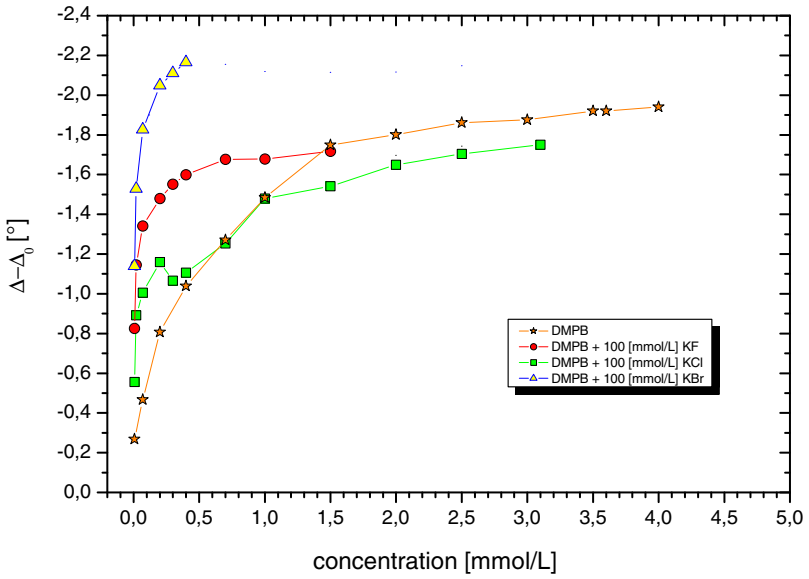

Figure 3.4: The ellipsometric angle $\Delta - \Delta_0$ as a function of the concentration of the surfactant. The ellipsometric angle Δ was subtracted by the one of a bare air/water interface Δ_0. The values for the pure solution and the solution where fluoride was added are significantly lower in comparison to the number density measured by SHG. A comparison leads to the fraction of condensed counterions in the compact layer at the interface. [1]

concentration with an independent technique. The desired quantity $\Gamma(c)$ is, for instance, given by the derivative of the surface tension isotherm or alternatively by the square root of the SHG signal. A Fresnel analysis proves a linear relation between the prevailing surface coverage and the ellipsometric angle Δ provided that there are no changes in the ion distribution with an increase of the surface concentration. Hence, a linear relation can be established if all counterions are located in the diffuse layer and a linear relation holds if all ions are condensed. As a next step measure the ellipsometric isotherm. Deviations from the linearity of the simulated $\Delta(\Gamma)$ dependence can be attributed to changes in the counterion distribution and yield directly the effective surface charge (see section 2.4.4). The corresponding plot

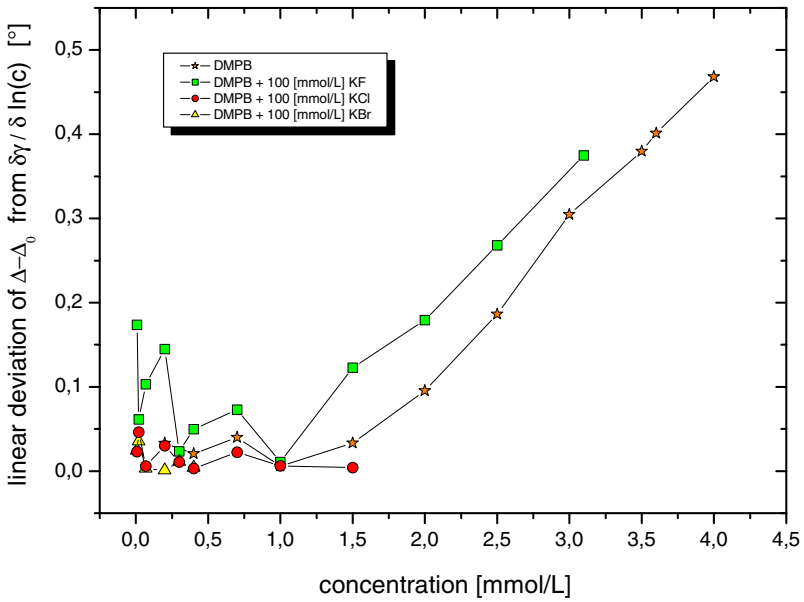

Figure 3.5: The ellispometric signal $\Delta - \Delta_0$ changes in a linear fashion with the surface coverage if all ions remain in the diffuse layer. Deviation of the measured ellipsometric signal $\Delta - \Delta_0$ from the corresponding simulated dependence with a fixed ion distribution indicate changes in the ion distribution. [1]

is given Figure 3.5 showing the deviation of the measured ellipsometric signal $\Delta - \Delta_o$ from the simulated one with a fixed ion distribution. The deviations are very pronounced for the pure surfactant and the surfactant solution with added fluoride ions. Both show a semi-quantitative agreement. For these two cases the data clearly indicate a redistribution of the counterions in the sublayer with increasing surfactant concentration. The addition of chloride and bromide leads immediately to a condensed state at all concentrations, and the ellipsometric data match the simulated dependence with all counterions condensed.

As shown in section 2.4.4 further quantification of the linear deviations yields the charge per molecule as a function of the number density of adsorbed

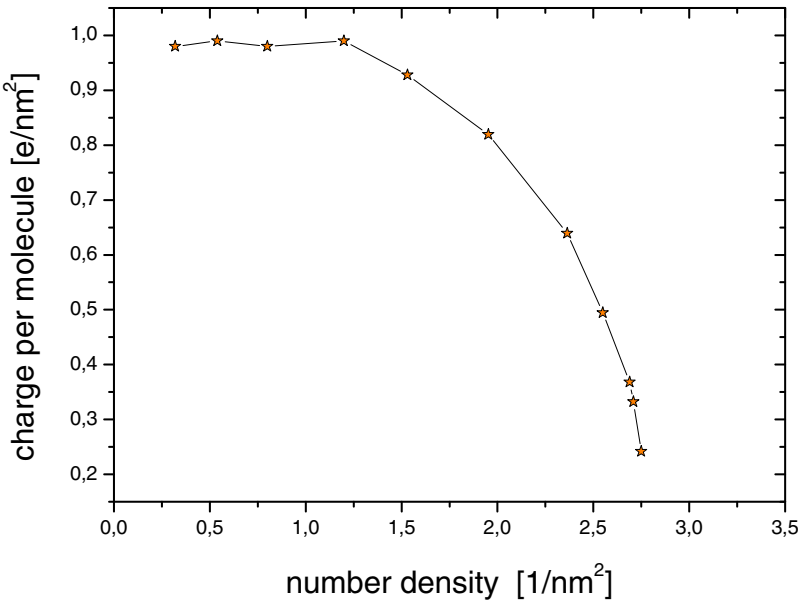

Figure 3.6: Charge per molecule as a function of the number density of adsorbed surfactants without any added electrolyte. A charge per molecule of one means that all counterions are located in the diffuse layer, a value of zero implies that all counterions are condensed. The plot reveals a sharp transition between a free and condensed state within a narrow concentration regime. [1]

surfactants without any added electrolyte as plotted in Figure 3.6. A charge per molecule of one means that all counterions are located in the diffuse layer; a value of zero implies that all counterions are condensed. The plot reveals a sharp transition between a free and a condensed state within a narrow concentration regime.

The observed ion specificity as well as the condensation cannot be captured by a pure electrostatic theory and is the manifestation of a subtle interplay of several competing evenly matched interactions. A similar ion specificity has been identified in the counterion binding of bromide and chloride ions to micellar solutions of hexadecyltrimethylammonium choride and

bromide. NMR investigations reveal a pronouncedly preferential binding of Br- ions to spherical and rodlike micelles [6, 7].

3.1.5 IR-VIS SFG measurements

In the previous section we provided direct experimental evidence for an unusual phase transition in an adsorption layer of the cationic surfactant 1-dodecyl-4-dimethylaminopyridinium bromide, at the air- water interface. Both surface phases differ in the distribution of the ions. At lower concentration the majority of counterions is spread out in a diffuse layer, whereas at higher concentrations the counterions are condensed. Such a phase transition is not captured by Poisson-Boltzmann type mean-field theories but is predicted if fluctuations are explicitly taken into account. In the next section infrared-visible sum frequency generation (IR-VIS SFG) spectroscopy was used to study the structure of the interfacial water and the vibrational alkyl stretching modes of both distinct surface phases. The vibrational signatures of both phases show striking differences and are used for obtaining a molecular picture. Furthermore the influence of an indifferent electrolyte on both surface states is investigated.

3.1.6 Interfacial water - a sensitive probe for the distribution of counterions

The vibrational spectrum of water is sensitive to the local molecular environment. The water vibrational spectrum probes the structure and energy of the hydrogen bonding network at the interface. In Figure 3.7 the IR-VIS SFG spectrum of a neat air-water interface is shown. The broad band peak from approximately 3000 to 3600 cm^{-1} is mainly consisting of two subbands centered around 3200 and 3450 cm^{-1} that can be attributed to OH stretching modes for water molecules in a broad distribution of tetrahedral bonding environments, both symmetric and asymmetric. The peak around 3200 cm^{-1} is comparable in frequency to the IR and Raman spectra of ice. It is related to strong intermolecular in-phase hydrogen bonds of water molecules that give rise to a highly correlated hydrogen-bonding network. The spectrum represents a continuum of OH symmetric stretches, ν_1 of water molecules in a symmetric environment. The higher energy broad band region of 3250-3500

cm^{-1} is assigned to weakly correlated OH stretching modes of molecular water that encompass both ν_1 (OH symmetric stretch) and to a lesser extent ν_3 (OH asymmetric stretch) vibrational modes. These water molecules reside in a more asymmetrically bonded water environment. The interpretation of the bound OH stretching modes is still an issue of controversy and requires further theoretical modeling. The absorption band at 3700 cm^{-1} corresponds to the free OH bond of the interfacial water.

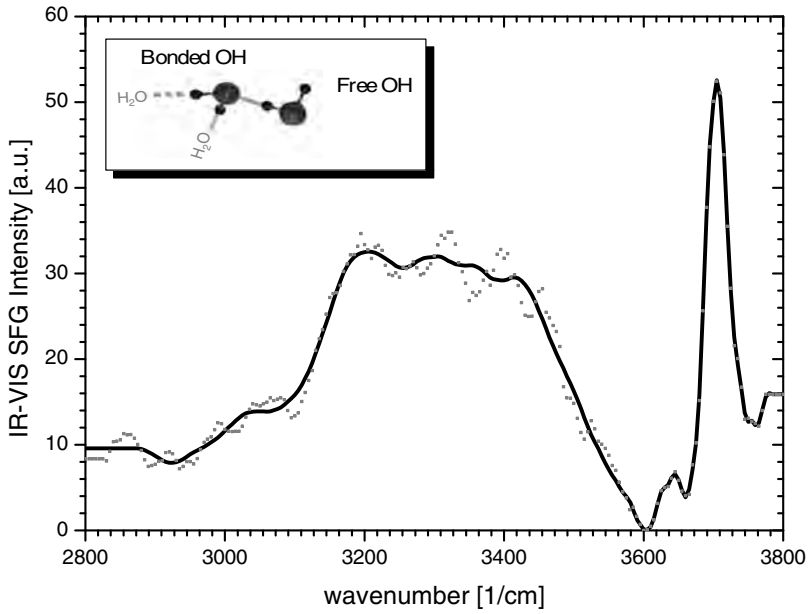

Figure 3.7: IR-VIS SFG spectrum of the air water interface recorded under *ssp* polarization. [8]

The IR-VIS SFG spectra of the soluble cationic amphiphile 1-dodecyl-4-dimethylaminopyridinium bromide, C12-DMPB at a concentration just below the cmc (4 mmol/l) is shown in Figure 3.8 (grey line). The black line represents the corresponding IR-VIS SFG spectra after adding 100 mmol/L KBr.

By adding 100 mmol/L of KBr to the surfactant solution the amount of counterions is increased by two decades. SHG measurements reveal that

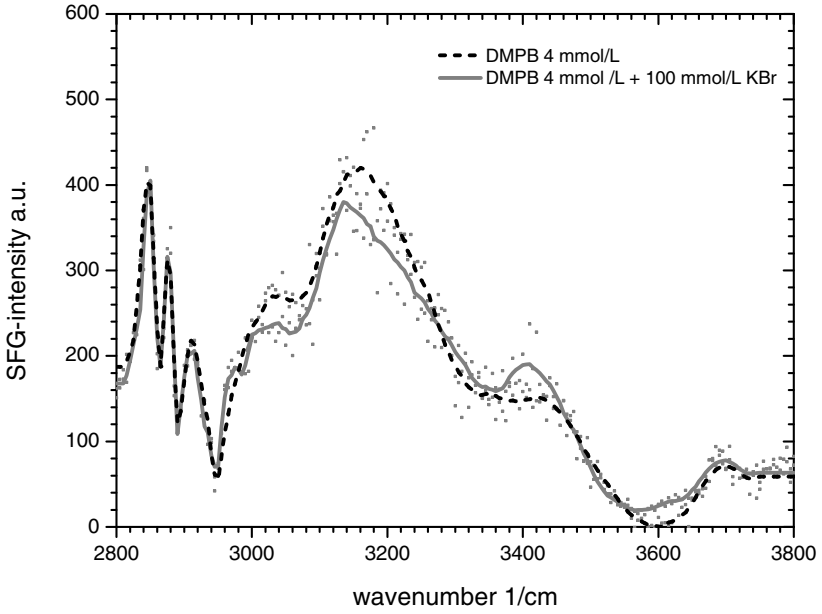

Figure 3.8: IR-VIS SFG spectra of C_{12}-DMPB at the air-water interface covering the alkyl and water vibrational stretching modes. The grey curve corresponds to a surfactant concentration of 4.0 mmol/L. The black line reflects the spectral changes after adding 100 mmol/L KBr. Only minor differences are observed which is in full agreement with a condensed state of the counterions before adding KBr. [8]

the number density of surfactants at the interface is not changed by the salt (KBr) (Figure 3.3). This is also evident by analyzing the intensity of the CH_2 and CH_3 stretching modes of the alkyl tail. The spectrum shows only minor changes in the region of 2800 to 3000 cm^{-1} upon salt addition.

The first prominent feature is an increase of the intensity of the bound OH stretching modes by a factor of ten for both solutions as compared to the IR-VIS SFG spectra of the neat air-water interface (Figure 3.7). The intensities of all spectra presented in this paper have been measured under identical settings and can be directly compared. The increase in the intensity in the spectral region of 3000-3600 cm^{-1} can be attributed to the oriental

order of the water dipoles induced by the electrostatic field at the interface and the increased probing depth.

The electrolyte is expected to cause dramatic changes in the spectra, if the surfactant follows the classical Poisson-Boltzmann picture. The electrolyte decreases the Debye-Hückel screening length by a decade [9, 10, 11]. As a consequence, a significant decrease of the vibronic intensities of bound water is expected. However, the experiment reveals only minor changes! The spectra with and without electrolyte differ by less than 10 per cent. This finding can only be understood if the counterions are already in a condensed surface state prior to the addition of KBr. The electrolyte KBr has then only a minor impact as represented in Figure 3.8.

The situation is completely different at lower concentration. According to the SHG and ellipsometry analysis, the majority of ions is then located in a diffuse layer according to Figure 3.6. As a consequence the electrolyte KBR should induce significant structural changes which are indeed observed in the corresponding IR-VIS SFG spectra. Figure 3.9 represents the IR-VIS SFG spectra of C12-DMPB at the air-water interface at surfactant concentration of 0.5 mmol/L (black line) and upon adding the electrolyte KBr (grey). Both spectra show striking differences, the intensity of the bound water bands decreases by about 50 percent due to the presence of the electrolyte. The changes are a direct consequence of the reduction of the Debye-Hückel screening length and the probing depth. Both factors reduce the number of water molecules contributing to the spectra.

The ion condensation at the air/water interface is revealed in the vibrational spectra of the water molecules. The contribution of bound OH-vibrations is considerably reduced due to the ion condensation. The structure of the interfacial water is an important aspect which is not yet properly addressed in current theories. It is also a sensitive probe for the prevailing surface state.

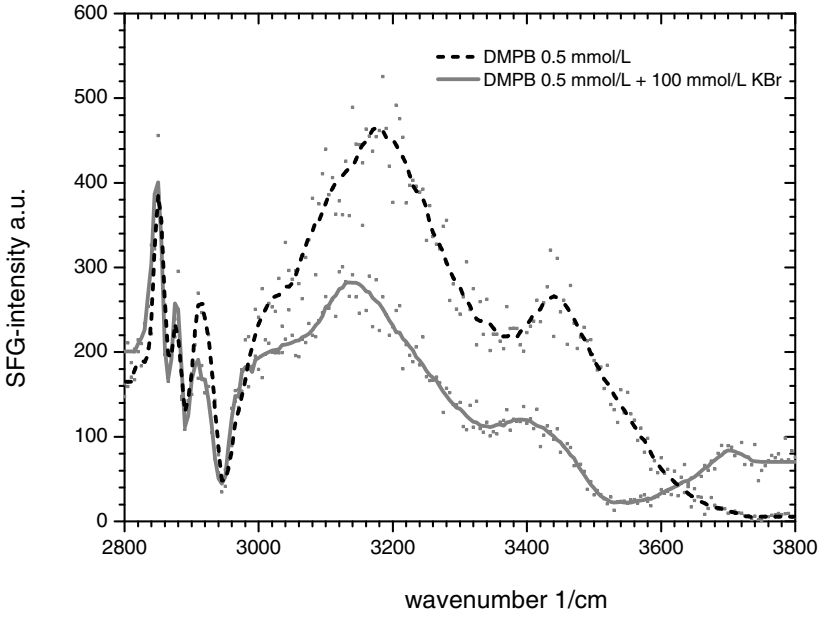

Figure 3.9: IR-VIS SFG spectra of C_{12}-DMPB at the air-water interface covering the alkyl and water vibrational stretching modes. The black curve corresponds to a surfactant concentration of 0.5 mmol/L. The grey line reflects the spectral changes after adding 100 mmol/L KBr. The striking differences are in accordance with a non-condensed state of the counterions before adding KBr. [8]

3.1.7 Conclusions: Ion distribution at charged interfaces

The influence of an indifferent electrolyte on the adsorption behavior of a cationic soluble surfactant has been investigated by surface tension measurements, ellipsometry, surface SHG and IR-VIS SFG. Each technique probes different structural elements, and the combination of all the techniques provides a profound picture of the interfacial architecture. The combined data shows the existence of a phase transition between a free and a condensed state in the distribution of the counterions. At higher bulk concentrations close to the cmc the counterions are condensed whereas at lower concentrations they are located in the diffuse layer. Addition of bromide and chloride leads to a condensed state at all concentrations whereas the addition of fluoride slightly shifts the phase transition to a lower concentration.

The number density and the surface excess at the cmc are equal for the pure solution and for the solution with added counterions of the same species, whereas the surface tension of the surfactant with the added counterions is significantly lower. This finding is currently investigated by molecular dynamic simulations.

The analysis of the data provides evidence for an ion-specific effect which cannot be categorized according to the periodic table of elements. Fluoride has an exceptional role in our measurements and is depleted on the surface. A finding which is as well observed by molecular dynamics simulations of simple salt solutions [12, 13, 14].

Additionally investigations of the structure of water by IR-VIS SFG also reveal the phase transition. At higher bulk concentrations the counterions are condensed whereas at lower concentrations they are located in the diffuse layer. Consequently, the IR-VIS spectra measured at the cmc are not changed by the electrolyte, however, striking differences are observed at lower concentrations. Recent work in our laboratory reveals that this behaviour is not limited to C12-DMPB and appears to be a general feature of cationic surfactants. The structure of the interfacial water is an important aspect which is not yet properly addressed in current theories. It is also a sensitive probe for the prevailing surface state.

Bibliography

[1] Koelsch, P.; Motschmann, H. *Langmuir*, in press

[2] R. Teppner, K. Haage, D. Wantke, H. Motschmann *J. Phys. Chem. B*, **104**, 11489, (2000)

[3] Adamson, A.W. *Physical Chemistry of Surfaces* (Wiley & Sons, New York, 1993).

[4] S. Bae, K. Haage, D. Wandtke, H. Motschmann *J. Phys. Chem. B.* **103(7)**, 1045-1050, (1999)

[5] H. Motschmann, R. Teppner "Ellipsometry in Interface Science", *Novel methods to Study Interfacial Layers*, edited by R. Miller, D. Moebius, Elsevier (2001)

[6] H. Fabre, N. Kamenka, A. Khan, G. Lindblom, B. Lindman, G. Tiddy J. Phys. Chem. **1980**, *84* 3428.

[7] J. Ulmius, N. Lindman, G. Lindblom, T. Drakenberg. J. Colloid and Interace Science,**1978**, *65*, 88.

[8] Koelsch, P.; Motschmann, H. *Langmuir*, submitted

[9] Gouy; G. *J. Phys.*, **1910**, *9*, 457.

[10] Chapman, D.L. *Phil. Mag.*, **1913**, *25*, 475.

[11] Stern, O. *Z. Elektrochem.*, **1924**, *30*, 508.

[12] P. Jungwirth and D.J. Tobias. *J Phys Chem B* 106 (2002), p. 6361.

[13] P. Jungwirth and D.J. Tobias. *J Phys Chem B* 105 (2001), p. 10468.

[14] P. Jungwirth, J.E. Curtis and D.J. Tobias. *Chem Phys Lett* 367 (2003), p. 704.

3.2 Foam stability

3.2.1 Relating foam stability and surface dilational rheology

The surface dilational elasticity modulus E of a soluble cationic surfactant at the air-water interface is measured in a frequency range of 1 Hz to 500 Hz. The data are then correlated with the lifetime of a foam lamella formed with the same surfactant solution. The surface rheological measurements have been performed with an improved design of the oscillating bubble technique (see section 2.5) that measures precisely the real and imaginary part of the complex dilational modulus E. The imaginary part captures a dissipative process which is interpreted as a surface dilational viscosity κ. The cationic surfactant 1-dodecyl-4-dimethylaminopyridinium bromide shows a transition between a surface elastic to a visco-elastic behavior with an increase of the bulk concentration. The transition corresponds to a striking increase in the lifetime of the foam lamella. The lamella lifetime of the visco-elastic system exceeds the one of an elastic system by two orders of magnitude while the absolute value of the E-modulus remains comparable. The results suggest that the intrinsic surface dilational viscosity κ is crucial for the ability of a surfactant system to form a stable foam. A simple picture that explains this observation is discussed.

The IR-VIS SFG spectra of the interfacial water provide a molecular interpretation of the underlying dissipative process connected to the intrinsic surface viscosity.

3.2.2 Lifetime of a foam lamella

The lifetime of a single foam lamella as a function of bulk concentration has been measured by the protocol mentioned above. The lifetime of a foam lamella depends critically on the bulk concentration with a pronounced transition between stable and unstable foam lamellae as shown in Figure 3.10 for C12-DMPB. At a concentration of $4.0 \cdot 10^{-3}$ mol/L the lifetime of the lamella is on the order of 400 seconds. It decreases with the bulk concentration and

is less than one second below a concentration of $0.7 \cdot 10^{-3}$ mol/L. Thus the foam lamella is stable at intermediate concentrations well below the cmc of $4.0 \cdot 10^{-3}$ mol/L.

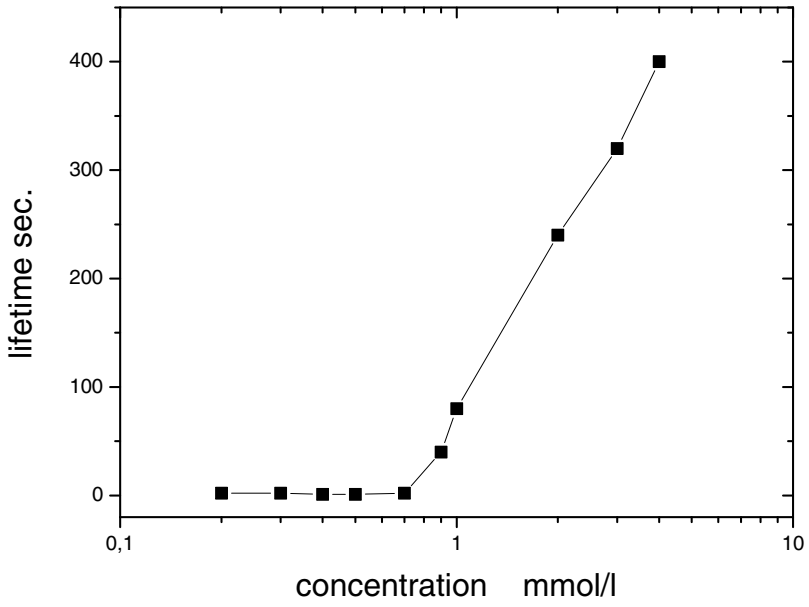

Figure 3.10: The lifetime of a foam lamella of aqueous solutions of the cationic surfactant C12-DMPB as a function of bulk concentration c. [1]

3.2.3 Oscillating bubble measurement

The surface dilational properties of both systems have been measured with the oscillating bubble technique in the frequency range of 1 - 500 Hz. The extended frequency range of our arrangement is of particular importance for the investigation of soluble amphiphiles because it captures the high frequency limit as discussed in 1.2.3

Figure 3.11 shows the magnitude of the complex modulus E for the C12-DMPB at a concentration of $4.0 \cdot 10^{-3}$mol/L just below the cmc (squares). The magnitude of the modulus increases at higher frequencies. In combi-

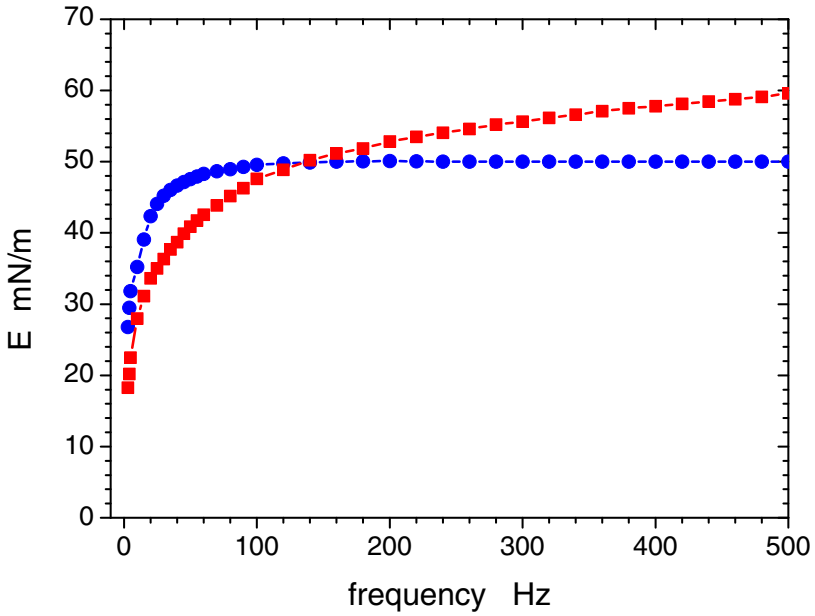

Figure 3.11: Magnitude of the complex modulus E of aqueous solutions of the cationic surfactant C12-DMPB as a function of the frequency ω of the bubble oscillation. The squares have been measured at a bulk concentration of $4.0 \cdot 10^{-3}$mol/L, the circles at a concentration of $0.7 \cdot 10^{-3}$mol/L. There is a transition between a purely elastic to a surface visco-elastic behavior. [1]

nation with a nonvanishing phase shift as described below this is a typical response of a surface visco-elastic layer. In eq 1.15 it is stated that the complex modulus E has two components. The first term accounts for the changes in the surface composition while the second term accounts for the frequency dependent contribution of the surface dilational viscosity κ to the E-modulus. According to the Lucassen-van den Temple-Hansen model the compositional term levels off into a plateau at higher frequencies. Under these conditions, the adsorption layer of the soluble surfactant behaves as a Langmuir layer of an insoluble amphiphile. The second term increases in a linear fashion with the frequency. The combined contribution reflects the measured frequency dependence of the magnitude of the complex modulus

E in Figure 3.11.

The picture changes completely at lower concentrations. The circles display the magnitude of the complex modulus E at $0.7 \cdot 10^{-3}$mol/L. It levels off into a plateau at frequencies higher than 100 Hz as predicted by the Lucassen-van Temple-Hansen model. Hence, the surface layer at the lower concentration behaves purely elastic at higher frequencies.

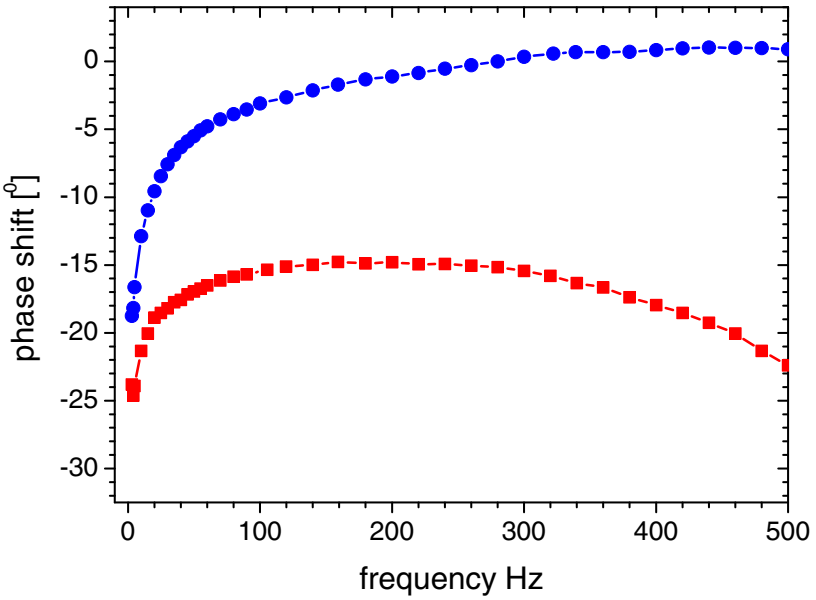

Figure 3.12: Phase shift ϕ between the sinusoidal piezo oscillation and the sinusoidal pressure response as a function of the frequency ν of the bubble oscillation. The triangles have been measured at a bulk concentration of C12-DMP of $4.0 \cdot 10^{-3}$mol/L, the squares at a concentration of $0.7 \cdot 10^{-3}$mol/L. A vanishing phase shift at higher frequencies indicates a purely surface elastic behavior. [1]

The transition from a visco-elastic to an elastic state is also reflected by the phase angle ϕ between the sinusoidal piezo and sinusoidal pressure signals as shown in Figure 3.12. At higher frequencies the intrinsic surface viscosity leads to a phase shift between both signals whereas a vanishing

phase shift ϕ is the distinct feature of a purely elastic component. Here the system response is immediately transferred to the pressure sensor as there is no dissipative process within the interfacial region.

The crossover between a surface elastic and a visco-elastic behavior at higher frequencies is reflected in a dramatic change of the corresponding lifetime measurements of an individual foam lamella as shown in Fig. 3.10. The data correlation suggests that the ability to form a stable foam lamella is linked to the intrinsic surface dilational viscosity κ.

The magnitude of the modulus $|E|$ remains comparable for the elastic and inelastic case. The SHG measurements as discussed in 3.1.3 reveal that the surface coverage changes by a factor of three between both concentrations. This goes along with a dramatic change in the foam stability.

There is a simple physical picture which supports our finding. A foam lamella ruptures because of mechanical disturbances. The details of the rupture mechanism are complex and several scenarios are discussed in the literature [3]. A surface viscosity locally damps the mechanical waves. The energy is dissipated in the surface layer and consequently the life time of the foam lamella is increased.

An intrinsic surface viscosity is connected to a dissipative process. Interfacial water is a sensitive probe for the energetic surrounding and is investigated by IR-VIS SFG in the next section

3.2.4 IR-VIS SFG measurements

The IR-VIS SFG spectra of C12-DMPB at two different concentrations are shown in the Figure 3.13. The most surprising feature is the fact, that the free OH peak is not present at the low concentration of C12-DMPB (c = 0.5 mmol/L) whereas it is clearly detectable at the higher concentration (c = 4 mmol/L) just below the cmc. Pure water has a sharp free OH peak at 3700 cm^{-1} (Figure 3.7), this peak is missing at an intermediate concentration of the surfactant and has a revive at the higher concentration. The breaking of the hydrogen bonding network of water costs energy. This dissipated energy can be interpreted as the molecular origin of the existence of an intrinsic surface viscosity consistent with the oscillating bubble experiments where only the higher concentration shows a surface visco-elastic behavior.

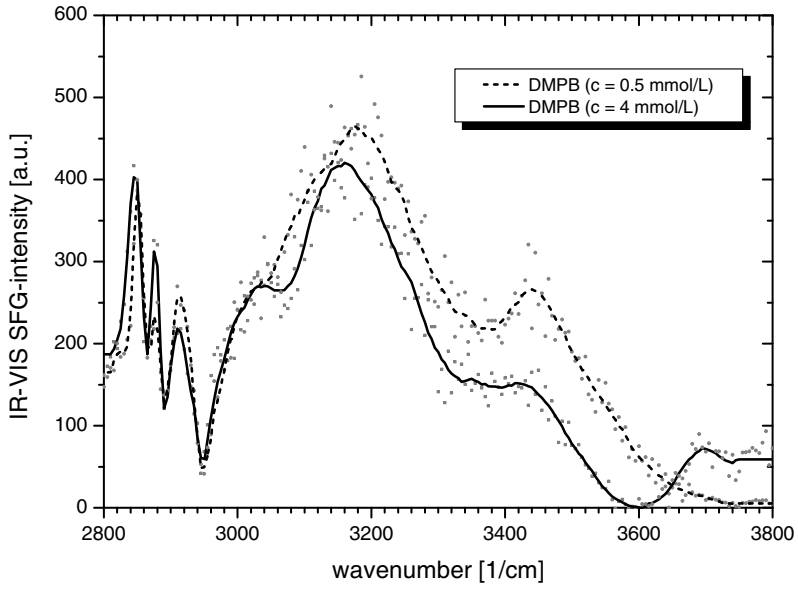

Figure 3.13: IR-VIS SFG spectra of C_{12}-DMPB at the air-water interface covering the alkyl and water vibrational stretching modes. The dotted curve corresponds to a surfactant concentration of 0.5 mmol/L and the black curve a concentration at the cmc of 4 mmol/L. The free OH-peak is suppressed at the lower concentration and has a revive at the higher concentration. [2]

One of the decisive processes in Gibbs monolayers is the molecular exchange of the adsorbed amphiphiles with those in the adjacent sublayer. To prove if the exchange process effectively causes the breaking of the hydrogen bonding network of water we investigated a Langmuir monolayer of the insoluble C20 amphiphile of the homologous series of this surfactant. The number density of the Langmuir monolayer is given by the preparation conditions and was carefully adjusted to match the prevailing one of the soluble surfactant at the higher concentration (c = 4 mmol/L). Figure 3.14 shows the corresponding IR-VIS SFG spectra. Obviously, there is no free OH peak detectable at the interface of the insoluble surfactant. Hence the exchange process of the adsorbed surfactants with the adjacent sublayer is related to the existence of a free OH-peak in the IR-VIS SFG spectra.

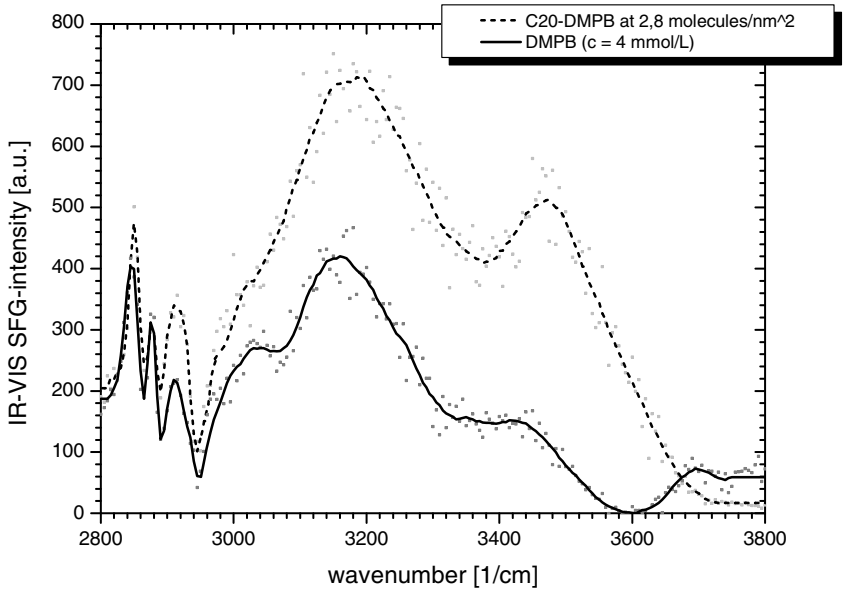

Figure 3.14: IR-VIS SFG spectra of the insoluble C20-DMPB amphiphile of the homologous series (dotted curve) with the same number density at the interface as the soluble C_{12}-DMPB amphiphile (solid line) at a concentration of 4 mmol/L. Even though the number density is comparable for both interfaces the free OH peak is only present when there is an exchange of surfactants at the interface with those in the bulk (solid line). [2]

3.2.5 Conclusions: Foam stability

In section 3.2.3 the complex surface dilational modulus E of a cationic surfactant is investigated in an extended frequency range of 1 Hz to 500 Hz with a novel version of an oscillating bubble device. The aqueous surfactant system shows a crossover from a surface elastic to a visco-elastic behavior with a moderate increase of the bulk surfactant concentration. The magnitude of the E modulus remains in both cases comparable. The measurements reveal that a surface viscosity is mandatory for the ability of the system to form a stable foam lamella. The surface viscosity damps mechanical distortions which otherwise may cause a rupture of the lamella. Hence, we are able to correlate the intrinsic surface dilational viscosity and the stability of a foam lamella.

The oscillating bubble technique in the presented version enables precise measurements of the complex E-modulus in a broad frequency range. The measurement is fast and convenient and determines the high frequency limit of the E modulus. Hence, the technique has the potential to be accepted as a new standard technique in Colloid and Interface science.

In section 3.2.4 the molecular origin of the dissipative process leading to a surface viscosity is investigated by IR-VIS SFG of the interfacial water. The free OH-peak of the bare air/water interface is suppressed by the surfactants at an intermediate concentration which corresponds to a surface elastic system. At an increased concentration corresponding to a surface visco-elastic system a revive of the free OH-peak in the IR-VIS SFG spectra is observed.

In order to relate the breaking of the hydrogen bonding network and the molecular exchange process the IR-VIS SFG spectra of the C20 representative of the homologous series of the surfactant is measured for the same surface coverage as the visco-elastic system. Since there is no exchange of adsorbed surfactants in this system the free OH-peak should be absent which is indeed the case. The creation of free OH-groups costs energy which can be interpreted as the dissipative process connected to the surface intrinsic viscosity. Hence, this interpretation provides an understanding of the stability of a foam lamella on the molecular scale.

Bibliography

[1] Koelsch, P.; Motschmann, H. *Langmuir*, submitted

[2] Koelsch, P.; Motschmann, H. *J. Phys. Chem. B*, submitted

[3] A. Vrij *Discuss: Faraday soc. 42* 1966, 23.

3.3 Combining static and dynamic properties

The aim of this last chapter is to bridge the static and dynamic properties of Gibbs monolayers. Figure 3.15 shows the SHG measurements for the solution of C12-DMPB in absence and in present of 100 mmol/L KBr. The addition of KBr at a concentration well below the cmc (0.5 mmol/L) leads to full monolayer coverage with the same number density at the interface as the pure C12-DMPB at the cmc (4 mmol/L). In both cases the counterions in the sublayer are condensed.

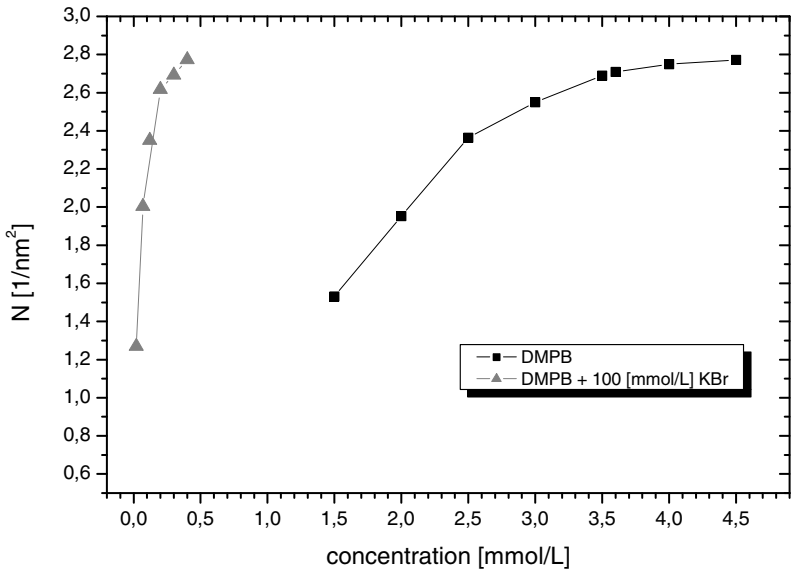

Figure 3.15: Number density of the surfactants measured by surface second harmonic generation. The black squares correspond to an aqueous solution of C12-DMPB and the gray triangles to a solution of C12-DMPB where 100 mmol/L KBr was added. The number density at the cmc for the pure solution is equal to the one where KBr was added.

Measurements of the lifetime of the foam lamella for an 8 times lower bulk concentration of the surfactant but with the same number density at the interface reveal comparable results:

	C12-DMPB	C12-DMPB + KBr
Bulk concentration of C12-DMPB	4 mmol/L	0.5 mmol/L
Number density at the interface	2.8 molec./nm^2	2.8 molec./nm^2
Lifetime of foam lamella	320 sec.	312 sec.

Table 3.1: Lifetime of a foam lamella at the cmc for C12-DMPB and C12-DMPB + 100 mmol/L KBr

In section 3.2.1 it is shown that the prerequisite for forming stable foam lamellae is the exsistence of an intrinsic surface viscosity. Therefore we should effectively observe a transition between a complete elastic system for the pure concentration of 0.5 mmol/L to a surface visco-elastic system where 100 mmol/L KBr is added to the solution. This is indeed the case as shown in Figure 3.16. The complex E-modulus shows all indications of an intrinsic surface viscosity for the solution with the added salt. The absolute value of the E-modulus is not leveling off into a plateau at higher frequencies and the phaseshift adopts values above 20° for the solution where KBr was added.

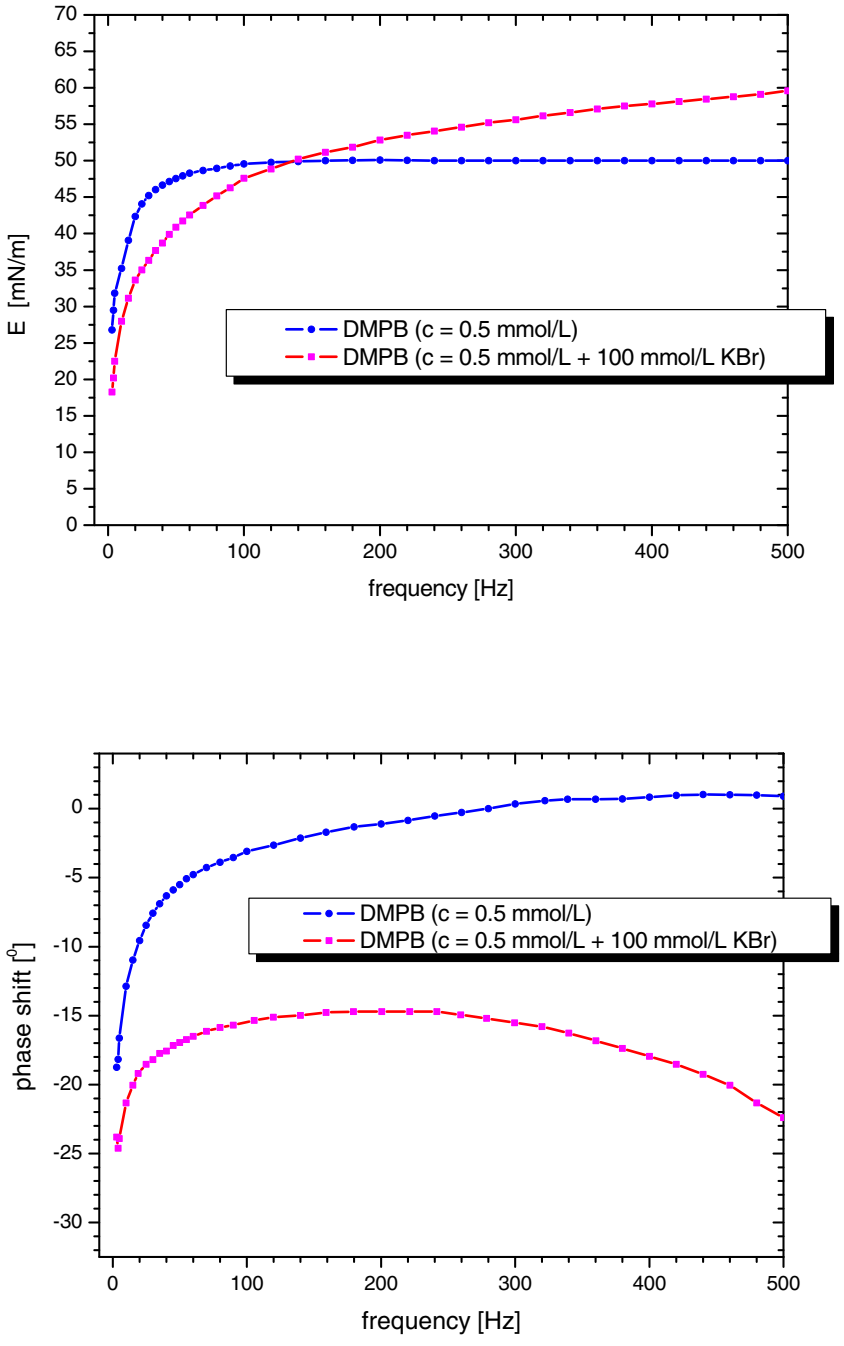

Figure 3.16: Complex modulus E and phase shift as as a function of the frequency ω of the bubble oscillation. The blue line corresponds to an aqueous solutions of the cationic surfactant C12-DMPB at a concentration of 0.5 mmol/L and the pink line to the same surfactant concentration where 100 mmol/L of KBr was added. The number density at the interface is increased by the addition of counterions, and the solution forms stable foam lamellas.

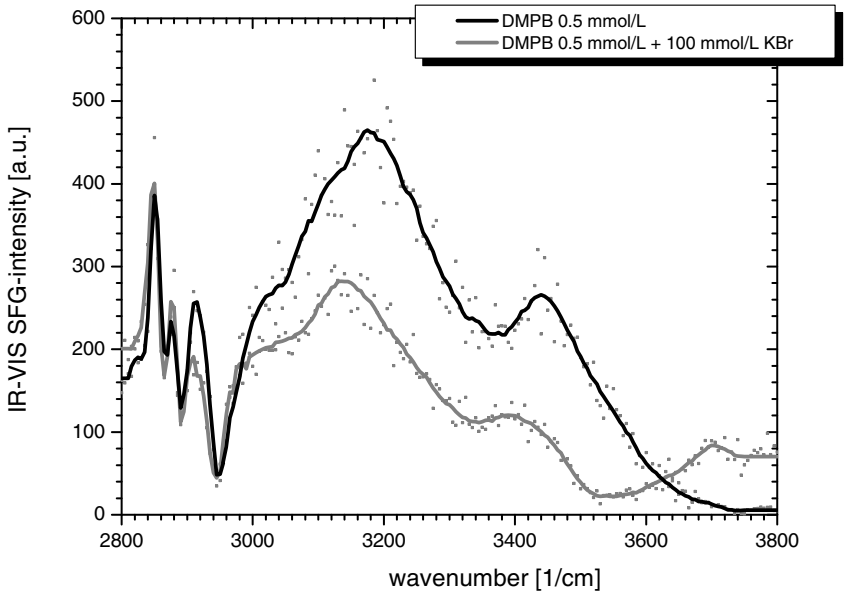

Figure 3.17: IR-VIS SFG spectra of C12-DMPB at the air-water interface covering the alkyl and water vibrational stretching modes. The black curve corresponds to a surfactant concentration of 0.5 mmol/L and the gray curve the same concentration with 100 mmol/L KBr added to the solution. Only for the solution with the added counterions the free OH-peak located at 3700 cm^{-1} is detectable.

The molecular origin of the intrinsic surface viscosity is related to the breaking of OH-bonds due to the exchange of surfactants in the bulk with those adsorbed at the interface as discussed in 3.2.4. Since the addition of salt increases the lifetime of the foam lamella and the surface changes to a visco-elastic system we should consequently observe a free OH-peak in an IR-VIS SFG spectrum only for the solution with the added KBr. The corresponding spectra are shown in Figure 3.17. The free OH-stretching mode is located at approximately 3700 cm^{-1} and is only present for the solution where KBr was added. Hence, the breaking of the hydrogen bonding network can be interpreted in terms of the dissipated energy connected to the surface intrinsic viscosity.

This chapter reveals the powerful possibilities in studying Gibbs monolayers combining static and dynamic properties of such interfaces with IR-VIS SFG. The water hydrogen bonding network plays a crucial role in understanding macroscopic phenomena on a molecular scale. This observational fact is not captured by the common theories and deserves much more attention.

This thesis reveals the following findings:

Ion distribution at charged interfaces

- Charged ionic surfactant can serve as model system for the investigation of the distribution of counterions at a charged interface.
- The combination of several optical techniques probing selectively different parts of the interface provides a detailed picture of the interfacial architecture.
- Ellipsometry and IR-VIS SFG are sensitive to the distribution of counterions in the sublayer.
- The impact of different counterions in the sublayer on the ellipsometric angle is quantified. A simple recipe is given for the interpretation of ellipsometric isotherms which can be used to retrieve the effective surface charge density.
- The combination of ellipsometry and surface SHG allows the determination of the distribution of counterions in the sublayer.
- The combined optical data show the existence of a phase transition between a free and a condensed state in the distribution of the counterions within a small increase of surface charge. This phase transition cannot be described by classical mean field theories and is not seen in Monte Carlo simulations.
- Addition of bromide and chloride anions leads to a condensed state at all surface charges.
- Fluoride has no propensity for the interface and consequently the addition of fluoride has minor effects on the counterion distribution in the sublayer.

Foam stability

- The method of the oscillating bubble allows the determination of the complex elasticity modulus of Gibbs monolayers in a frequency range from 1-500 Hz. This is an increase of about two decades to the conventional bubble and drop shape analysis tensiometry.
- The extension in the frequency range allows to measure the high frequency limit of the complex elasticity modulus.
- A nonvanishing phase shift at higher frequencies indicates a surface visco-elastic behavior.
- The existence of an intrinsic surface viscosity is a prerequisite for the formation of a stable foam lamella.
- The molecular origin of the dissipative process leading to a surface viscosity is investigated by IR-VIS SFG.
- Gibbs monolayers which behaves completely elastic at higher frequencies suppress the existence of free OH groups at the interface.
- Surface visco-elastic systems shows a pronounced free OH-peak in the IR-VIS SFG spectrum.
- The creation of free OH-groups costs energy which can be interpreted as the dissipative process connected to the surface intrinsic viscosity.
- The decisive processes is the molecular exchange of the adsorbed amphiphiles with those in the adjacent sublayer. This exchange process effects the breaking of the hydrogen bonding network at the interface.

3.4 Outlook

After more than a century the mysterious trends of the Hofmeister series challenge scientists on a interdisciplinary level. A compilation of Collins and Washabaugh from 1984 [1] mentioned well over 30 properties of salt solutions that show systematic differences with ionic, particular anionic type: The stability, precipitation and solubility of proteins; transport, spectral and thermodynamic properties of water and salt; solution surface potentials and surface tensions, to name a few. The present theories are not capable to describe these effects in a predictive theory due to the zoo of complicated interactions present in these systems. Interfaces are playing an important role in this processes. Further experimental studies measuring density profiles perpendicular to the interface and coupling these experimental studies with theoretical efforts and molecular dynamics simulations are therefore highly desirable.

Simple salt solutions are raising the surface tensions compared to pure water. A subsequent thermodynamic treatment would imply, that the ions are repelled from the interface. Recent molecular dynamics simulations challenge this view. In simulations of a 6 M aqueous NaCl solution, 10 to 15 % of the accessible surface area was occupied by chloride ions, whereas sodium was effectively excluded from the topmost liquid layer. In their simulations of sodium halide solutions, Jungwirth and Tobias [2, 3] observed an increase in surface concentration with increasing size and polarizability of the halide ion. Thus, fluoride is depleted at the interface, whereas chloride and bromide concentrations are enhanced, a trend which is consistent to the observations with surfactant covered interfaces in this thesis. However, the simulations are sensitive to the description of the molecular interactions they employ [4]. Therefore, direct experimental observations of molecular structure and energetics of ions in the interfacial region are needed to corroborate the simulations. Using the strategies reviewed in this thesis, IR-VIS SFG and ellipsometry has the potential to directly probe interfaces of simple salt solutions and give experimental evidence for the simulated density profiles across the interface.

In the same sense, a recent publication of Lau et.al [5] predict a first order phase transition for multivalent ions at very low surface charges (0.5 or less charges per nm^2), which could be again experimentally supported by

IR-VIS SFG measurements of surfactant covered surfaces at very low surface coverages as outlined in section 3.1.6.

The IR-VIS SFG spectra can theoretically be further analysed. The intensity depends on the amount of oriented water molecules in the vicinity of the interface. In a first simple approach the electric field distribution can assumed to be Poisson-Boltzmann like. Once the electric field is known, the average orientation of water dipoles can be calculated using a Langevin function. The convolution of this two function could then be fitted to the peak intensities of the IR-VIS SFG spectra and consequently be compared with corresponding molecular dynamics simulations.

In the context of foam stability it would be a roadmap to find a general correlation between the stability of a foam lamella and the intrinsic surface viscosity comparable to the correlation of foam formation and the relative dynamic surface pressure as depicted by von Rybinski et. al. [6]. It is therefore desirable to measure the complex dilatational modulus for a set of classical surfactant systems with the oscillating bubble device and to correlate the data with the lifetime of the corresponding foam lamellae. It would be as well challenging to study surfactant and/or protein mixtures and to further implement a new design of the capillary which enables studies at the oil-water interface.

Bibliography

[1] Collins,K.D; Washabaugh,Q.; *Rev.Biophys.* **1985**, *18*, 323.

[2] P. Jungwirth and D.J. Tobias. *J Phys Chem B* 105 (2001), p. 10468.

[3] P. Jungwirth and D.J. Tobias. *J Phys Chem B* 106 (2002), p. 6361.

[4] Dang , L.X.; Chang,T.M.; *J Phys Chem B* 106 (2002), p. 235.

[5] A.W.C. Lau, D.B. Lukatsky, P. Pincus, and S.A. Safran, *Phys. Rev. E* 65, 051502 (2002)

[6] Engels, Th., von Rybinski, W., Schmiedel, P., Progr. Coll. Polym. Sci., **111**, 117, (1998)

Acknowledgment

This work has been performed at the Max-Planck-Institute of Colloids and Interfaces in Potsdam. First of all I would like to thank the head of the department, Prof. Helmuth Möhwald for his steady support and fruitful discussions, and for valuable comments on the articles. It was a great pleasure to be a part of the interface department with all the scientific opportunities.

Dr. Hubert Motschmann was the supervisor in the field of research over this years. He introduced me to the field of Gibbs monolayers and nonlinear optical spectroscopy, ellipsometry, and the oscillating bubble device. He always supported me in many areas and shared his knowledge. It was a very fruitful teamwork with Hubert and a great pleasure for me working with him, and I likewise thank him for his warm hospitality.

Dr. Dieter Wantke for introducing me the field of surface rheology and discussions about the oscillating bubble experiment.

Audrée Andersen from the 'Gibbs Monolayer group' and all other PhD-students and members of the interface department of the Max-Planck-Institute for lively discussions and cooperations.

Annemarie Martins for preparing solutions and performing surface tension measurements. Gabriele Wienskohl for her patience on the oscillating bubble experiment. She did a great job in operating this new experimental setup. Ingeborg Bartsch for a helping hand in the laboratory work. Andreas Kretzschmar for designing various holders and the nitrogen floated box for the nonlinear optical experiments as well as the oscillating bubble device. Wolfgang Stein for his support in the electronic workshop and Cliff Janiszewski for the preparation of glass capillaries.

Prof. Pavel Jungwirth for the cooperation and sharing ideas which were effectively influencing the work related to the ion distribution.

Prof. Werner Kunz and Prof. Barry Ninham for the workshop entitled 'Short Range Interactions in Soft Condensed Matter - from Solutions to Materials and Biological Systems' held in Regensburg 2004 and the related stimulating discussions.

Prof. Mark Rutland and Prof. Robert Pugh for the NLO-meeting in Stockholm and Eric Tyrode for sharing technical information with other groups using nonlinear optics.

Walfred and Angelika Siebel, Odina Kölsch and Jorit Pfleiderer for their support and confidence on my scientific work.